1) IONIZED ABSORBERS IN ACTIVE GALACTIC NUCLEI

2) VERY STEAP SOFT X-RAY QUASARS

NASA Grant NAG5-3039

Final Report

For the Period 15 August 1995 through 14 February 2000

Principal Investigator
Dr. Fabrizio Fiore

November 2000

Prepared for:

National Aeronautics and Space Administration
Goddard Space Flight Center
Greenbelt, Maryland 20771

Smithsonian Institution
Astrophysical Observatory
Cambridge, Massachusetts 02138

The Smithsonian Astrophysical Observatory
is a member of the
Harvard-Smithsonian Center for Astrophysics

The NASA Technical Officer for this grant is Dr. Nicholas White, Code 668, Laboratory for High Energy Astrophysics, NASA/Goddard Space Flight Center, Greenbelt, Maryland 20771.

Final report on grant NAG5-3039

Grant NAG5-3039 includes the proposals:

1. The Complex X-ray Spectrum of Quasars with Soft Excess

2. Ionized Absorbers in AGN

3. Very Steap Soft X-ray Quasars

The activity concerning the three proposal ended.

A paper presenting the results of the ASCA observation of NGC985 has been published on The Astrophysical Journal (Nicastro, Fiore & Matt 1999, ApJ, 517, 108) and on the proceedings of the Conference "The Active X-ray sky" (Nicastro, Fiore, Brandt & Reynolds, 1998, Nuclear Physics B, 69/1-3 (1998) 501. This observation showed the importance of resonant absorption in modifying the 0.5-1.5 keV spectrum of this source. Detailed physical models have been produced.

The ASCA observations of the two Soft X-ray Quasars PG1244+026 and NAB0205+024 have been published on the Montly Notices of the Royal Astronomy Society (Fiore et al. 1998, MNRAS, 298, 103). A spectral feature at about 1 keV has been discovered in PG1244+026, similar to those in other steep X-ray spectrum Seyfert 1 galaxies and quasars. The line could result from reflection from an highly ionized disk, in line with the view that steep X-ray spectrum AGN are emitting close to their Eddington luminosity.

The papers quoted above are attached to this report.

Best Regards,

Fabrizio Fiore

Mon. Not. R. Astron. Soc. 298, 103–113 (1998)

ASCA observations of two steep soft X-ray quasars

F. Fiore,[1,2,3] G. Matt,[4] M. Cappi,[5,6] M. Elvis,[3] K. M. Leighly,[6,7] F. Nicastro,[1,8] L. Piro,[8] A. Siemiginowska[3] and B. J. Wilkes[3]

[1] *Osservatorio Astronomico di Roma, Via dell'Osservatorio, I-00044 Monteporzio Catone, Italy*
[2] *SAX Science Data Center, Via Corcolle 19, I-00131 Rome, Italy*
[3] *Harvard–Smithsonian Center of Astrophysics, 60 Garden Street, Cambridge, MA 02138, USA*
[4] *Dipartimento di Fisica, Università degli Studi 'Roma Tre', Via della Vasca Navale 84, I-00146 Rome, Italy*
[5] *Istituto per le Tecnologie e Studio Radiazioni Extraterrestri (ITESRE), CNR, via Gobetti 101, I-40129 Bologna, Italy*
[6] *Cosmic Radiation Laboratory, RIKEN, Hirosawa 2-1, Wako-shi, Saitama 351, Japan*
[7] *Columbia Astrophysics Laboratory, Columbia University, 538 West 120th Street, New York, NY 10027, USA*
[8] *Istituto di Astrofisica Spaziale (IAS), CNR, Via E. Fermi 21, I-00044 Frascati, Italy*

Accepted 1998 February 27. Received 1998 February 24; in original form 1997 September 7

ABSTRACT

Steep soft X-ray (0.1–2 keV) quasars share several unusual properties: narrow Balmer lines, strong Fe II emission, large and fast X-ray variability, and a rather steep 2–10 keV spectrum. These intriguing objects have been suggested to be the analogues of Galactic black hole candidates in the high, soft state. We present here results from *ASCA* observations for two of these quasars: NAB 0205 + 024 and PG 1244 + 026.

Both objects show similar variations (factor of ~2 in 10 ks), despite a factor of ~10 difference in the 0.5–10 keV luminosity (7.3×10^{43} erg s^{-1} for PG 1244 + 026 and 6.4×10^{44} erg s^{-1} for NAB 0205 + 024, assuming isotropic emission, $H_0 = 50.0$ and $q_0 = 0.0$).

The X-ray continuum of the two quasars flattens by 0.5–1 going from the 0.1–2 keV band towards higher energies, strengthening recent results on another half-dozen steep soft X-ray active galactic nuclei.

PG 1244 + 026 shows a significant feature in the '1-keV' region, which can be described either as a broad emission line centred at 0.95 keV (quasar frame) or as edge or line absorption at 1.17 (1.22) keV. The line emission could be a result of reflection from a highly ionized accretion disc, in line with the view that steep soft X-ray quasars are emitting close to the Eddington luminosity. Photoelectric edge absorption or resonant line absorption could be produced by gas outflowing at a large velocity (0.3–0.6 c).

Key words: line: formation – line: identification – galaxies: individual: NAB 0205 + 024 – galaxies: individual: PG 1244 + 026 – galaxies: Seyfert – X-rays: galaxies.

1 INTRODUCTION

The *ROSAT* Position Sensitive Proportional Counter (PSPC) has found a large spread in the energy spectral indices of low-z quasars[1]: $0.5 < \alpha_{0.1-2\,\mathrm{keV}} < 3.5$. In about 10 per cent of cases $\alpha_{0.1-2\,\mathrm{keV}} \gtrsim 2$ (e.g. Laor et al. 1994, 1997; Walter & Fink 1993; Fiore et al. 1994). The large spread in $\alpha_{0.1-2\,\mathrm{keV}}$ favoured the discovery of its correlation with other properties. In fact, the steep soft X-ray quasars have then been realized to share a cluster of unusual properties:

(i) narrow Balmer lines[2] (Laor et al. 1994, 1997; Boller, Brandt & Fink 1996);

(ii) strong Fe II emission (Laor et al. 1994, 1997; Lawrence et al. 1997);

(iii) rapid, large-amplitude variability – factor of 2–50 on time-scales from minutes to months (Boller et al. 1996; Brandt, Pounds & Fink 1995; Otani, Kii & Miya 1996; Boller et al. 1997);

(iv) somewhat steep hard X-ray spectra, $2 > \alpha_{2-10\,\mathrm{keV}} > 0.6$ (Pounds, Done & Osborne 1995; Brandt, Mathur & Elvis 1997).

Pounds et al. (1995) suggest the latter to be a close physical analogy with the X-ray power law produced by Comptonization in a hot accretion disc corona in Galactic black hole candidates (BHCs) in their 'soft, high' state. This is not the only analogy between BHCs and steep X-ray spectrum quasars. Laor et al. (1994, 1997) explained the correlation with Hβ full width at half-maximum (FWHM) to be the result of the larger size of a virialized broad emission-line region for an active galactic nucleus (AGN) in a high L/L_{Edd} state. Ebisawa (1991) found that, while the soft component

[1] We use 'quasars' to describe broad line emission objects, regardless of luminosity.

[2] The permitted lines have FWHM $\lesssim 2000$ km s^{-1}, yet still are clearly broader than the forbidden lines.

of six BHC observed by *Ginga* is roughly stable on time-scales of 1 day or less, the hard component exhibits large variations down to millisecond time-scales. These time-scales translate to 10^4 yr and 0.1 d for quasars, if they scale with the mass of the compact object. The soft component of a BHC extends up to ~10 keV in a BHC in 'soft, high' states, and it is often associated with optically thick emission from an accretion disc. If this is the case, the temperature should scale with the mass of the compact object as $M_{BH}^{-1/4}$, and the above energy translates to 0.1–0.4 keV for quasars. The rapid large-amplitude variability shown by a few narrow-line Seyfert 1 galaxies (NLSy1s) at about 1 keV on time-scales of hours to days (Otani et al. 1996; Brandt et al. 1995; Boller et al. 1997) can then be analogous to the above BHC hard component flickering.

A steep X-ray spectrum quasar with 10–100 times the luminosity of NLSy1s should be larger and so should vary no more rapidly than several days. Instead Fiore et al. (1998) find that steep X-ray spectrum PG quasars commonly vary by a factor of 2 in one day. Variability therefore seems to be correlated with X-ray spectral slope and Balmer linewidth (and therefore possibly with the accretion rate) rather than with the luminosity.

Evidence for spectral features in the '1-keV' region in many steep soft X-ray quasars is building up (Turner et al. 1991; Brandt et al. 1994; Otani et al. 1996; Comastri, Molendi & Ulrich 1995; Leighly et al. 1997, in preparation). Instead, 'normal' Seyfert 1 galaxies (having broad Balmer lines and flatter soft X-ray spectra) usually have their strongest absorption features at lower energies (in the 0.6–0.9 keV 'oxygen' band). An intriguing possibility is that the appearance of these features at different energies also depends on L/L_{Edd}.

Detailed high-energy X-ray spectra of luminous quasars with steep soft X-ray spectra are essential to understand the 'narrow–broad line' phenomenon in AGN, in particular whether the peculiar X-ray properties depend on optical luminosity, on optical-to-X-ray ratio (α_{OX}), or on their Eddington ratio. To this end we selected two bright quasars with $\alpha_{0.1-2\,keV} > 2.0$ (Fiore et al. 1994) at the extreme values of optical luminosity, both with low Galactic N_H (Table 1) of 1.9×10^{20} cm^{-2} for PG 1244 + 026 and of 3.0×10^{20} cm^{-2} for NAB 0205 + 024 (Elvis, Lockman & Wilkes 1989) and observed them with *ASCA* (Tanaka, Inoue & Holt 1994). We report the results in this paper.

2 OBSERVATION AND DATA REDUCTION

Table 1 gives the redshift, M_V, the 0.2–2 keV luminosity, α_{OX}, the average PSPC count rate and spectral index and the Galactic N_H for the two quasars. Table 2 gives the *ASCA* observation log, the SIS and GIS exposure times and count rates.

Both observations were performed in two charge-coupled device (CCD) mode with the source at the 'ICCD mode' position. Data reduction was performed using FTOOLS 3.6. We used 'bright' mode SIS data, combining low, medium and high bit rates. Conservative cleaning criteria were applied (minimum Earth occultation = 7°, minimum magnetic rigidity = 6 GeV/c, minimum bright Earth angle = 20°, and excluding data collected in the first 32 s after the satellite passage in the South Atlantic Anomaly (SAA) and through the day–night terminator). Counts, light curves and spectra from the two quasars were accumulated in circular regions of 3 and 4 arcmin radius for SIS and GIS respectively.

We are interested in the high-energy spectrum of these sources and since they are rather faint, and possibly very steep, background subtraction plays a crucial role. Background counts were accumulated from regions surrounding the sources and compared with counts accumulated from the same regions from 'blank-sky' observations. The 'local' and 'blank-sky' background counts were always within 10 per cent of each other for the four *ASCA* instruments. To obtain the best possible signal-to-noise ratio in the background-subtracted spectra, we therefore used the 'blank-sky' background in our spectral analysis. We extracted background spectra from 'blank-sky' event files using the same regions as for source extraction. The count rates of the two sources become that of

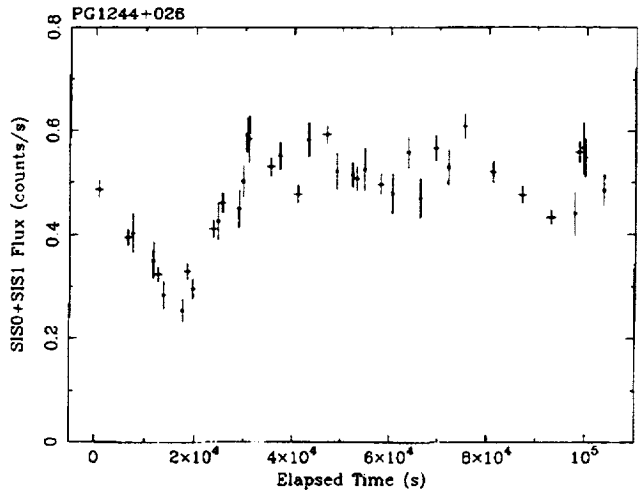

Figure 1. The SIS 0.5–7 keV light curve of PG 1244 + 026.

Table 1. Steep soft X-ray quasars.

name	z	M_V^a	$L_{0.2-2keV}$ 10^{45} erg s^{-1}	α_{OX}	PSPC cts/s	$\alpha_{0.1-2keV}$	$N_{H(Gal)}$ 10^{20} cm^{-2}
PG1244+026	0.048	−21.1	0.14	1.4	1.0	2.3±0.1	1.9[b]
NAB0205+024	0.155	−25.0	1.8	1.6	0.7	2.3±0.1	3.0[b]

[a] $H_0 = 50$, $q_0 = 0$. [b] Elvis et al. (1989).

Table 2. *ASCA* observations.

name	Dates	Exposure SIS-GIS ks	2 SIS count rate cts/s	2 GIS count rate cts/s
PG1244+026	1–3 Jul 1996	37–39	0.442+/−0.004	0.241+/−0.004
NAB0205+024	18–20 Jan 1996	50–54	0.150+/−0.001	0.153+/−0.002

the background at about 7 keV (observer frame). After background subtraction PG 1244 + 026 is observed in the GIS up to 10 keV and NAB 0205 + 024 up to 8 keV (9.3-keV quasar frame), both at the $> 3\sigma$ level.

Spectral fits were made separately to the spectra from the four *ASCA* instruments and to the spectra obtained combining together the data from the two SIS and GIS detectors. The results were consistent with each other. In the following we present the results obtained following the second approach. In some cases χ^2 are smaller than 1. This is because of the prescription adopted in adding the spectra, for the propagation of the errors (the Gehrels 1986 algorithm: error = 1.0 + SQRT(N + 0.75)). Spectra were always rebinned following two criteria: (a) to sample the energy resolution of the detectors with four channels at all energies where possible, and (b) to obtain at least 20 counts per energy channel. In the spectral fits we limited ourselves to the 0.6–10 keV energy band, to minimize the systematic effect caused by the uncertainty in the SIS calibration below 0.6 keV. N_H was always constrained to be greater than or equal to the Galactic value along the line of sight.

In all cases the quoted errors represent the 90 per cent confidence interval for one interesting parameter.

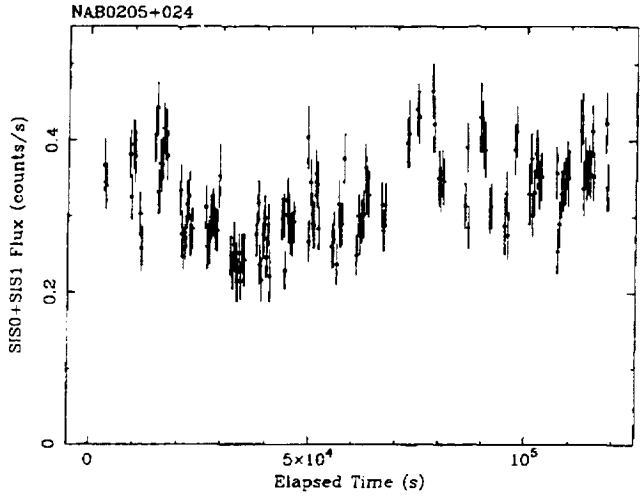

Figure 2. The SIS 0.5–7 keV light curve of NAB 0205 + 024.

3 VARIABILITY

ASCA observed the two quasars for a total elapsed time of 105 ks (PG 1244 + 026) and 119 ks (NAB 0205 + 024). We can therefore study the variability of these sources on time-scales from a few hundred seconds to about 1.5 d.

Figs 1 and 2 show the SIS light curves of the two sources. Following Ptak et al. (1994) the values were computed using variable bin sizes corresponding to good time intervals longer than 200 s.

Significant variations are evident in both light curves. A factor of 2 variability, both down and up, in about 10 ks is present at the beginning of the light curve of PG 1244 + 026. A drop of a factor of ~2 is present at the beginning of the light curve of NAB 0205 + 024 on a ~15-ks time-scale. In this paper we limit ourselves to pointing out that roughly similar variability is observed in two sources that differ in luminosity by a factor of ~10. Significant, although rather small, spectral variability is also present in the *ASCA* observations of the two sources. A systematic analysis of the variability in different energy bands and of the spectral variability is in progress and will be presented, together with a similar analysis on a sample of about 20 Seyfert 1 galaxies and quasars observed by *ASCA* and *BeppoSAX*, in a paper in preparation. In the following sections we present the average properties of the spectra. We anticipate that the spectral variability will not modify the results presented here.

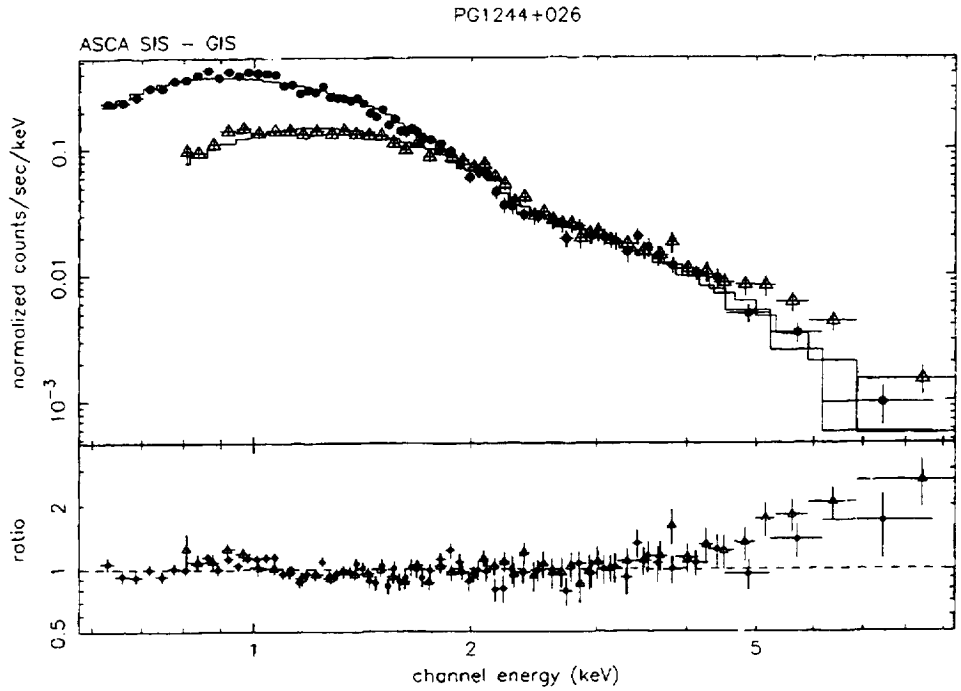

Figure 3. The SIS + GIS spectra of PG 1244 + 026 fitted with a simple absorbed power-law model. The lower panel shows the ratio between the data and the best-fitting model.

4 SPECTRAL ANALYSIS

Figs 3 and 4 show the SIS + GIS spectra of PG 1244 + 026 and NAB 0205 + 024 fitted with a simple power law absorbed at low energy by a column of cold gas equal to or higher than the Galactic column along the line of sight. Table 3 gives the best-fitting parameters and χ^2. It is clear that this simple model is inadequate to describe the 0.6–10 keV spectrum of both quasars. A hard tail, larger than the 5–10 per cent systematic uncertainties at these energies (Gendreau & Yaqoob 1997), is evident in both cases. In the spectrum of PG 1244 + 026 there is also a significant excess with respect to the model at about 1 keV. The feature is visible in both SIS and GIS detectors. We discuss these two findings in turn in the next two subsections.

4.1 The 0.6–10 keV continuum

The *ASCA* SIS and GIS responses are peaked at 1–2 keV and decrease sharply at higher energies. Therefore the *ASCA* '2–10 keV' slopes are strongly biased towards the lowest energy boundary. This means that some caution should be used when comparing *ASCA* '2–10 keV' slopes with those of experiments whose

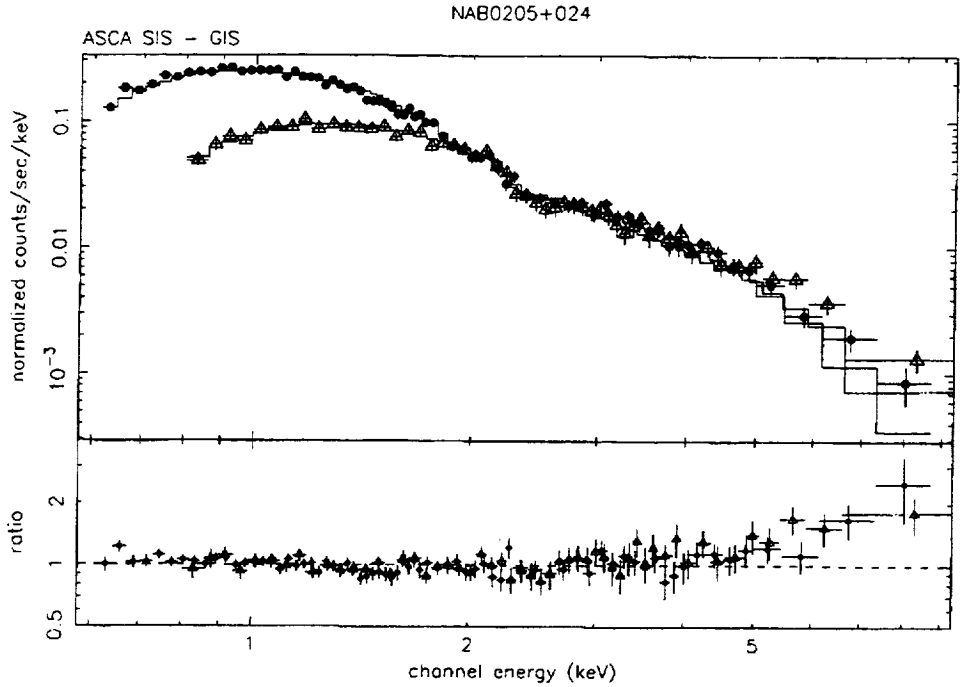

Figure 4. The SIS + GIS spectra of NAB 0205 + 024 fitted with a simple absorbed power-law model. The lower panel shows the ratio between the data and the best-fitting model.

Table 3. PG 1244 + 026 and NAB 0205 + 024 spectral fits.

model	N_H^a	α_E or T[b]	α_H or $\Omega/2\pi$	E^b_{break} or A[c]	χ^2 (dof)
PG1244+026					
PL 0.6-10 keV	1.9+0.6	1.67±0.04	–	–	177.9 (148)
PL 2-10 keV	1.9FIXED	1.35±0.12	–	–	48.4 (82)
PL 3-10 keV	1.9FIXED	1.03±0.30	–	–	29.1 (58)
PL 4-10 keV	1.9FIXED	0.67±0.55	–	–	14.4 (38)
Broken PL 0.6-10 keV	$3.6^{+2.6}_{-1.7}$	$180^{+1.1}_{-0.2}$	$1.06^{+0.24}_{-0.38}$	2.8±0.6	149.1 (145)
PL+Raym 0.6-10 keV	1.9+0.7	$0.88^{+0.2}_{-0.05}$	1.54±0.06	>0.5	135.3 (145)
PL+BB 0.6-10 keV	$5.3^{+8.0}_{-3.4}$	0.16±0.03	1.40±0.15	–	139.2 (145)
PL+Comp.Refl 0.6-10 keV	$2.6^{+1.3}_{-0.7}$	2.78±0.06	>8	–	150.5 (146)
NAB0205+024					
PL 0.6-10 keV	3.0+0.1	1.38±0.02	–	–	126.2 (147)
PL 2-10 keV	3.0FIXED	1.09±0.10	–	–	42.4 (86)
PL 3-10 keV	3.0FIXED	0.94±0.20	–	–	23.3 (58)
PL 4-10 keV	3.0FIXED	0.62±0.45	–	–	9.5 (38)
Broken PL 0.6-10 keV	3.0+1.4	$1.50^{+0.3}_{-0.1}$	0.98±0.10	2.4±0.5	85.2 (145)
PL+Raym 0.6-10 keV	3.0+7.0	0.49±0.05	1.02±0.25	<0.01	82.8 (144)
PL+BB 0.6-10 keV	3.0+0.2	0.16±0.02	1.15±0.07	–	86.2 (145)
PL+Comp.Refl 0.6-10 keV	3.0+0.2	1.44±0.04	>4.2	–	95.2 (146)

[a] In 10^{20} cm^{-2}. [b] In keV. [c] Metal abundances.

responses peak around 6 keV, such as *EXOSAT*, *Ginga*, *BeppoSAX* and *XTE*. To address this, we fitted the SIS + GIS spectra of PG 1244 + 026 and NAB 0205 + 024 with a simple power law in the observed 0.6–10, 2–10, 3–10 and 4–10 keV ranges. The results are given in Table 3 and shown in Fig. 5.

In the last three series of fits N_H was fixed to the Galactic value. The best-fitting slopes flatten by 0.5–1 going from the low energy to the higher energy range. (We note that for NAB 0205 + 024 the quasar redshift implies that these slopes refer to slightly harder energy ranges: 10 keV in the observer frame corresponds to 11.6 keV in the quasar frame).

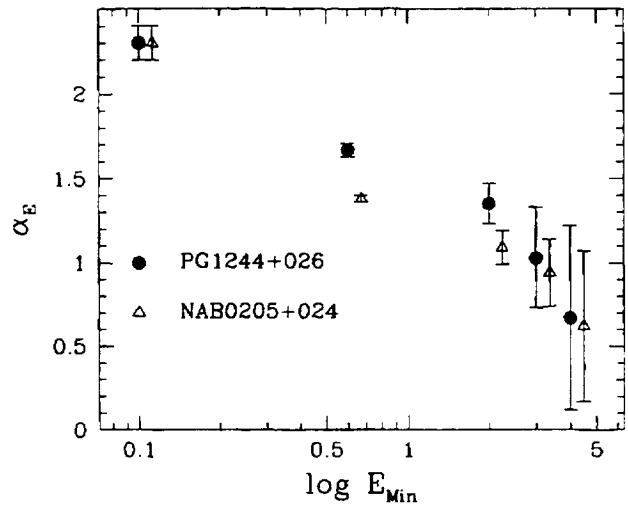

Figure 5. The PG 1244 + 026 (filled circles) and NAB 0205 + 024 (open triangles) best-fitting power-law index in the observed 0.6–10, 2–10, 3–10 and 4–10 keV ranges as a function of the range minimum energy. The NAB 0205 + 024 points have been shifted from real energy for the sake of clarity. The PSPC 0.1–2 keV points are also shown for comparison.

The PSPC spectral index for both quasars is 2.3 ± 0.1 (Fiore et al. 1994), steeper than any of the values in Table 3. For NAB 0205 + 024 the *ASCA* low-energy index is flatter than the PSPC by 0.4–0.8, and the *ASCA* best-fitting N_H coincides with the Galactic value, suggesting that the spectrum continues to steepen below *ASCA* X-ray energies.

To parametrize a curved spectrum we have also fitted the 0.6–10 keV spectra of the two quasars with: a broken power-law model; a power law plus optically thin plasma emission (Raymond & Smith 1977) model; a power law plus blackbody model; a power law plus Compton reflection model. The results are again shown in Table 3 and confirm the presence of significant curvature in the spectra of these quasars.

In PG 1244 + 026 the power law plus Raymond–Smith model gives a χ^2 significantly better than the broken power-law model because it also fits the ~1-keV feature (see next subsection). However, the best-fitting energy index is still very steep and positive residuals are evident above 4 keV (Fig. 6). In NAB 0205 + 024 the power law plus Raymond–Smith model gives an acceptable χ^2 only for low metal abundances, given the absence of significant features in the spectrum, similar to the *ROSAT* results of Fiore et al. (1994). Above 4 keV the best fit is similar to that in the broken power-law model. Fits with a power law plus blackbody model give acceptable χ^2 in both cases. The power-law indices in this case are slightly steeper than in the broken power-law model. Inspection of the residuals shows again a slight excess of counts at high energy. In PG 1244 + 026 the power law plus blackbody model again gives a χ^2 significantly better than the broken power-law model because it partly fits also the feature around ~1 keV (see next subsection). Fits with a Compton reflection model (PLREFL in XSPEC) give χ^2 significantly higher than the previous models and push the parameter $\Omega/2\pi$ to high and implausible values.

We do not see any significant line emission at the energies of the iron Kα lines. The 90 per cent upper limits to the equivalent width of a narrow line at 6.4 (and 6.7) keV, rest frame, in

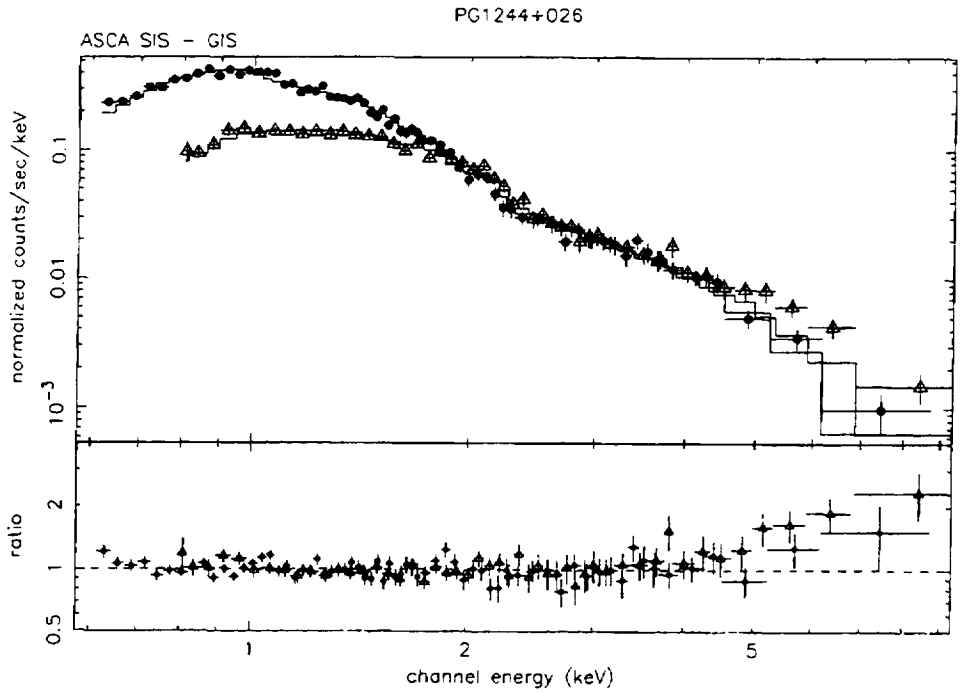

Figure 6. The SIS + GIS spectra of PG 1244 + 026 fitted with a power law + Raymond–Smith model. The lower panel shows the ratio between the data and the model.

PG 1244 + 026 and NAB 0205 + 024 are 400 and 230 eV (640, 314 eV) respectively.

The χ^2 for the fits to the PG 1244 + 026 spectra are much higher than those for the similar fits to the NAB 0205 + 024 spectra because of the presence of the '1-keV' feature in the former quasar. We discuss this feature next.

4.2 Low-energy features

We have already noted that a '1-keV' feature seems to be present only in PG 1244 + 026, the quasar with the lower luminosity. Fig. 7 shows the results of a simple power-law model fit to the 0.6–4 keV spectrum of PG 1244 + 026: the '1-keV' feature is clearly visible.

It has recently been realized that Residual Dark Distribution (RDD; the error in *ASCA*'s onboard correction for CCD dark current) can affect the low-energy *ASCA* SIS spectra. The symptom of the RDD problem is a sudden decrease in the SIS effective area towards lower energies from about 1 keV. We are however confident that this has little effect on the '1-keV' feature, for the following reasons: (a) SIS data of PG 1244 + 026 and NAB 0205 + 024 have similar RDD value but the '1-keV' feature is visible in the spectrum of PG 1244 + 026 only. The 90 per cent upper limit to any unresolved Gaussian line emission at about 1 keV in NAB 0205 + 024 is of 20 eV. (b) The feature is present also in the GIS spectrum (c). The feature is present at the same level in SIS0 and SIS1, while the RDD tends to be greater for SIS1 than for SIS0.

To investigate the physical origin of the '1-keV' feature and to quantify its strength, we performed a series of spectral fits to the SIS and GIS spectra of PG 1244 + 026 using only the 0.6–4 keV range, to avoid the complications of the hard tail (see previous section). The results are reported in Table 4, along with those of the other fits in this section.

4.2.1 *Emission-line model*

The fit with a power-law model plus a Gaussian line gives a small χ^2 (90.1 for 101 degrees of freedom). The equivalent width of the 1-keV feature, in the power law plus Gaussian line fit, is similar in the SIS and GIS detectors. In Table 4 we report the SIS determination of 64 ± 15 eV. The linewidth is well constrained and cleanly resolved in the SIS spectrum to $\sigma = 0.11^{+0.01}_{-0.03}$ keV.

A fit with a power law plus a thermal plasma model (Raymond & Smith 1977) gives an acceptable χ^2 (93.1 for 100 d.o.f.). The best-fit temperature (1 keV) implies that the '1-keV' emission is dominated by a blend of iron L and neon emission lines.

An emission-line feature can be mimicked by fitting a spectrum with a strong absorption feature at slightly higher energies. We have then fitted the SIS and GIS spectra with models including absorption structures.

4.2.2 *Absorption-edge fits*

Fits with one absorption edge give χ^2 significantly higher than the previous case (102.5 for 102 d.o.f.). The edge energy (1.17 keV, quasar frame) is consistent with that of Ne IX and/or Fe L, Fe XVI and Fe XVII. The best-fitting neutral N_H is significantly higher than the Galactic value. This is reasonable, since if there is highly ionized Ne and Fe L absorption it is likely to have also highly ionized oxygen absorption at 0.74–0.87 keV. We then refitted the SIS and GIS spectra with a model including three absorption edges, at the energies of the most abundant ions in highly ionized gas with high Ne IX abundance, i.e. O VII, O VIII and Ne IX–Fe XVI–Fe XVII (Nicastro et al. 1998), fixing the cold N_H to the Galactic value. The results were not satisfactory. The depth of the oxygen edges is zero with small upper limits and χ^2 is significantly higher than in the previous case: 114.7. Leaving N_H free improves χ^2, but the oxygen

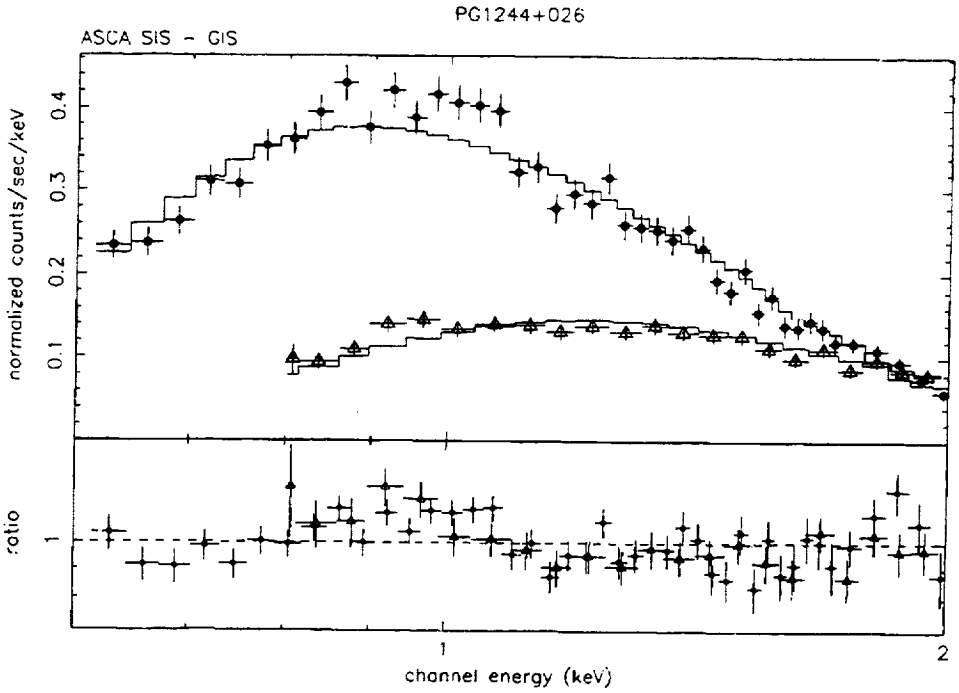

Figure 7. The SIS + GIS spectra of PG 1244 + 026 fitted in the 0.6–4 keV range. The lower panel shows the residuals when the spectrum is fitted with a simple absorbed power law.

Table 4. PG 1244 + 026: spectral fits in the band 0.6–4 keV.

Continuum models model	α_E	N_H^a	T[b]	A[c]		χ^2 (dof)
PL	1.70±0.02	1.9+1.0	–	–	–	131.8 (104)
PL+BB	1.50±0.11	9.5±5.0	0.14±0.02	–	–	109.5 (101)
PL+Raym	1.61±0.03	1.9+0.3	1.00+0.06	>0.5	–	93.1 (100)
emission line						
			line E[b]	line EW[d]		χ^2 (dof)
PL+Gauss	1.60±0.04	1.9+0.5	0.91±0.03	64±15	–	90.1 (101)
absorption edge models						
			edge E[b]	τ		χ^2 (dof)
PL+1 edge	1.88±0.11	8.2±3.0	1.12±0.03	0.25±0.07	–	102.5 (102)
PL+2 edges	1.88±0.11	1.9FIXED	1.12±0.10	0.26±0.08	–	94.8 (101)
			<0.64	0.51±0.14		
ionized absorber models						
			logN_H(ionized)	U or logT	z abs.	χ^2 (dof)
1-Phot. ion.	1.92±0.10	11.1±3.5	22.59±0.15	2.00±0.12	0.25±0.07	93.2 (101)
2-Phot. ion.	1.94±0.10	11.0±3.5	21.56±0.10	1.20±0.10	–0.33±0.10	95.7 (101)
3-Coll. ion.	1.90±0.10	11.3±3.5	22.62±0.14	6.92±0.07	0.24±0.06	90.7 (101)
absorption notch models						
			T[b], notch E[b]	notch width[d]	Cov. frac.	χ^2 (dof)
PL+notch	1.93±0.08	9.3±3.3	1.44±0.05	680±70	0.14±0.04	97.5 (100)
PL+BB+notch	1.48±0.20	7.8±4.4	T=0.16±0.03			97.1 (100)
			1.16±0.03	14±7	1FIXED	

[a] In 10^{20} cm^{-2}. [b] In keV. [c] Metal abundances. [d] In eV.

edge depths are still zero and the fit resembles completely the single-edge fit. Fixing N_H to the Galactic value but leaving free the energies of two edges again produces a good fit ($\chi^2 = 94.8$, 101 d.o.f.). The best-fitting energy of one edge is again 1.12 keV, but that of the other edge is < 0.64 keV (observer frame), close to the lower boundary of the observed range. So, if the cold absorption is fixed to the Galactic value, then there must be additional absorption edge(s) at energies lower than the observed range, corresponding to oxygen less ionized than O VI. We note, however, that this conclusion is weakened by the unknown contribution of the SIS RDD, which pushes low-energy events below the detection threshold.

A 1.17-keV absorption feature can also be interpreted in terms of blueshifted oxygen absorption (Leighly et al. 1997). In this case, assuming that the absorption is mostly due to O VIII, the shift from the quasar frame would be equivalent to $z = -0.38$. A more complex continuum has little effects on the best-fit parameters of absorption edges.

4.2.3 *Ionized absorber model fits*

We fitted the data with a detailed ionized absorber model (not including resonant scattering absorption lines). We first generated a grid of photoionization equilibrium models using CLOUDY (Ferland 1996), and fitted the spectrum interpolating by this grid, using the method of Fiore et al. (1993). To calculate the models we have assumed the observed spectral energy distribution (SED) (Fiore et al. 1995; Elvis et al. 1994). This is important, since the soft X-ray spectrum of this source strongly differs from that of 'normal' Seyfert 1 galaxies, where warm absorbers are usually found (Reynolds 1997). A steep soft X-ray spectrum can completely ionize oxygen and neon but not iron, and so can produce edges in the 1–2 keV (Fe L) and 7–9 keV (Fe K) ranges, but not in the 'oxygen' 0.6–0.9 keV band. A fit with this model produces an acceptable χ^2 (see Table 4, ionized absorber model 1).

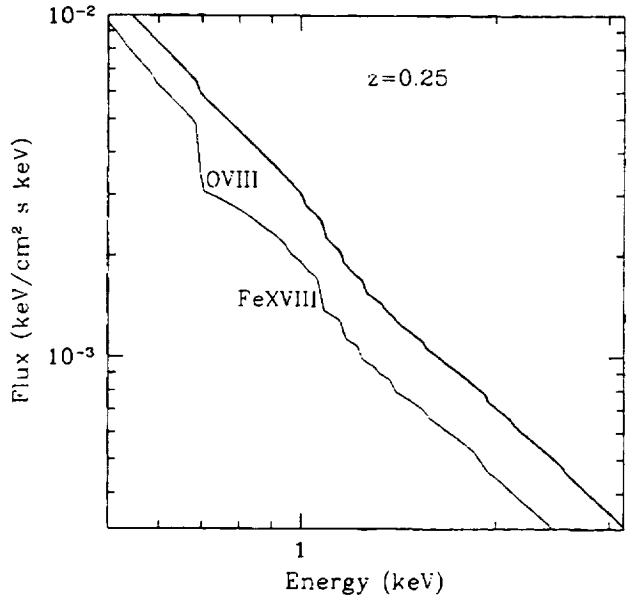

Figure 8. The thick line shows the best-fitting photoionized absorber model for PG 1244 + 026 using the observed steep spectrum (note that the absorber has $z = 0.25$, while the quasar has $z = 0.048$). The thin line shows a photoionization model obtained using a much flatter SED (see text). Both models produce Fe L absorption features around 1 keV. The flat SED also produces a deep O VIII edge, which is not observed.

In Fig. 8 we show the best-fitting steep SED model (thick line) and a photoionization model obtained using a standard, much flatter

AGN SED (a power law of $\alpha = 1.2$ from ultraviolet to X-rays, thin line), which, above 1 keV, gives a comparably good fit to the data. While iron in the flat SED model has an ionization structure similar to that of the model obtained using the right SED, oxygen is much less ionized: note the deep O VIII edge present in the flat SED model.

In this fit the redshift of the absorber is significantly higher than that of the quasar, because the main feature in the transmitted spectrum is the Fe XXVI edge at 1.36 keV, while the deepest edge in the quasar spectrum is at 1.17 keV (quasar frame). However, a good fit can also be obtained for a different absorber redshift ($z = -0.33$, Table 4, ionized absorber model 2). In this case the 1.17 keV feature is interpreted in terms of O VII and O VIII absorption. We cannot discriminate between these two solutions on statistical grounds.

We have also tried fits with a collisional equilibrium model (Nicastro et al. 1998). The results were very similar to those obtained in the case of photoionization equilibrium (see Table 4, ionized absorber model 3).

In all fits with detailed warm absorber models the column of cold gas is significantly higher than the Galactic value, similar to the values found using single edges to parametrize the absorber (Table 4).

4.2.4 *Absorption-line fits*

Fits with a single Gaussian absorption line do not give acceptable χ^2. Fits with two or more absorption Gaussian lines can produce χ^2 of 96 or smaller. These models are indistinguishable for the SIS from models with a broad absorption notch, which we discuss in the following. Physical models including resonant absorption lines, as well as absorption edges from ionized plasma, will be discussed in a future paper (Nicastro et al., in preparation).

4.2.5 *Absorption-notch fits*

Fits with an absorption notch give χ^2 higher than those with an emission line by $\Delta\chi^2 \approx 7$. While the power law plus notch fit is formally acceptable, the best-fitting value of the notch width is implausibly large (almost 1 keV), forced by the very low value of the covering fraction required by the fit. However, the notch best-fitting parameters are strongly dependent on the proper modelling of the continuum. For example, using a power law plus a blackbody to parametrize the continuum gives an acceptable fit fixing the notch covering fraction to 1, which in turn results in a much more reasonable value for the notch width of 14 ± 7 eV. The *ASCA* bandwidth is not wide enough and its spectral resolution is not good enough to constrain adequately *both* a complex continuum *and* the notch parameters.

4.2.6 *Comparison with the PSPC results*

PG 1244 + 026 was observed with the PSPC in 1991 December and the results of this observation have been reported by Fiore et al. (1994). The 0.6–2 keV flux level during the PSPC observation was about 50 per cent lower than the mean flux in the *ASCA* observation. The fit of an absorbed power law to the PSPC spectrum gives an acceptable χ^2 (22.8 for 25 d.o.f.), $\alpha_{0.1-2\,\mathrm{keV}} = 2.3 \pm 0.1$ and $N_{\mathrm{H}} = 2.9 \pm 0.3 \times 10^{20}$ cm^{-2}, slightly higher than the Galactic value. Most of the PSPC counts were detected below 0.3 keV, in the 'carbon' band. The quality of the spectrum between 0.3 and 2 keV is not very high and emission or absorption features fainter than ~20 per cent cannot be excluded in this energy band. No evidence of spectral variability is present in the *ROSAT* data despite a factor of 2 flux variability.

The PSPC data strongly constrain the level of any cold or warm absorption affecting the 'carbon' band. Best-fitting models to the *ASCA* data including absorption features in the 1–2 keV band (Table 4) require a rather large absorption in addition to the Galactic one below 1 keV. Therefore, it is important to study whether the *ASCA* best-fitting models are consistent with the PSPC ones. Rather than performing joint fits to the *ASCA* and PSPC data, which are complicated by the large uncertainty in the relative PSPC/*ASCA* SIS calibration, and by the detailed shape of the continuum over the broad 0.1–4 keV band, we fitted the PSPC data with a power-law model including the emission or absorption features found in the previous section (see Table 4). The results are shown in Table 5, where we also report (in brackets) the 99 per cent parameter upper limits, or confidence intervals, when appropriate.

We see that the presence of an emission line at 0.91 keV is not required by the PSPC spectrum, but an equivalent width of 65 eV is not excluded (10 per cent probability). However, the presence of a cold absorber of thickness $8.2 \pm 3.0 \times 10^{20}$ cm^{-2} is inconsistent with the PSPC spectrum (probability < 1 per cent), while the presence of an edge at 0.62 keV with $\tau = 0.51 \pm 0.14$ is only marginally consistent with the PSPC result.

5 DISCUSSION

5.1 Continuum

The *ASCA* observations of PG 1244 + 026 and NAB 0205 + 024 have shown that the X-ray continuum of these two quasars flattens by 0.5–1 on passing from the 0.1–2 keV (PSPC) to the 2–10 keV band. Similar results were obtained by Brandt et al. (1997); by Comastri et al. (1998) and Leighly et al. (in preparation) on TONS 180, by Pounds et al. (1995) and Fiore et al. (in preparation) on REJ 1034 + 390, and by Leighly et al. (in preparation) on AKN 564. It appears that the X-ray spectrum of a sizeable number of steep PSPC and narrow Balmer line quasars has significant curvature, being flatter at higher energies.

This could be a result of different components influencing the spectrum at different energies, as might happen in 'normal' broad-line Seyfert 1 galaxies and quasars, where a soft component is often present. The relative intensity of the two components would be

Table 5. PG 1244 + 026: spectral fits to the PSPC.

model	N_H^a	α_E	line or edge E[b]	line EW[c] or τ	χ^2 (dof)
PL	2.9±0.3	2.3±0.1			22.8 (25)
PL+gauss	2.9±0.3	2.3±0.1	0.91FIXED	0+68 (+100)	22.8 (23)
PL+1 edge	2.7±0.4(0.6)	2.2±0.2	1.12FIXED	$0.3^{+0.4}_{-0.3}$	20.9 (24)
PL+2 edges	2.7±0.4	2.2±0.2	1.12FIXED	$0.3^{+0.4}_{-0.3}$	20.9 (23)
			0.62FIXED	0+0.34 (+0.62)	

[a] In 10^{20} cm^{-2}. [b] In keV. [c] In eV.

quite different from 'normal' quasars. Laor et al. (1997) suggested a fainter hard component relative to the optical in the majority of low-redshift PG quasars (assuming a two-component model). However, Grupe (1996) found evidence for a stronger soft excess in a sample of soft X-ray selected Seyfert galaxies dominated by narrow-line objects.

A large relative intensity of the soft component has important consequences on various competing models for the soft component. Disc reprocessing models (Matt, Fabian & Ross 1993; Fiore, Matt & Nicastro 1997) would require highly anisotropic emission to account for the discrepancy between the observed soft and hard fluxes. Optically thin free–free emission (e.g. Barvainis 1993) is ruled out by these observations because the best-fitting power-law slope is still too steep to fit the spectrum about 4 keV, because variability rules out optically thin plasma (Elvis et al. 1991) and because of the implausibly low metal abundances (< 1 per cent solar, see Table 3) required in NAB 0205 + 024 (see section 3.2.1). The most likely origin for the steep component is Comptonized disc emission (e.g. Czerny & Elvis 1987; Fiore et al. 1995; Pounds et al. 1995).

The high-energy spectral index of the two quasars $\alpha_H \sim 1.0$ (see Table 3) is consistent with that of 'normal' Seyfert 1 galaxies (e.g. Nandra & Pounds 1994; Nandra et al. 1997). The error on α_H is however large and so no strong conclusion can be drawn on the origin of the hard emission. An answer to this question must await the large area and high energy sensitivity of *AXAF*, *XMM* and *Spectrum X-gamma*.

5.2 Origin of the ~1-keV feature in PG 1244 + 026

The ~1-keV feature in PG 1244 + 026 could be explained in terms of either a broad ($\sigma = 0.1$ keV) emission line at 0.91 keV (0.95 keV quasar frame) of about 60 eV equivalent width or a $\tau = 0.25$ absorption edge at 1.17 keV (or an absorption notch at 1.22 keV). These possibilities cannot be discriminated between on statistical grounds.

An absorption interpretation requires additional low-energy absorption, either cold (with a column density higher than Galactic by $\sim 7 \times 10^{20}$ cm^{-2}; see Tables 4 and 5), in contrast with the PSPC results, or a warm absorber with a peculiar ion abundance distribution.

The observed spectrum can be interpreted in terms of either an inflowing ($v/c = 0.25$) or an outflowing ($v/c = -0.33$) absorber. In the first case the ion contributing most to the absorption is Fe XVIII, and in the second case it is O VIII. The two cases cannot be discriminated between on statistical grounds. While an outflowing absorber has been suggested in several other cases (see e.g. Mathur et al. 1994), this would be the first case for an inflowing highly ionized absorber.

A similar situation is found in IRAS 13224 − 3809 by Otani et al. (1996), and in AKN 564 by Brandt et al. (1994) and Leighly et al. (in preparation). Otani et al. (1996) and Leighly et al. (1997) interpret the features in the 1–2 keV band in terms of blueshifted absorption from relativistically ($v = 0.2$–0.6 c) outflowing material. If the 1.17-keV feature in PG 1244 + 026 is due to a blueshifted O VIII photoelectric absorption, then the absorption seen below 0.64 keV may be due to C VI photoelectric absorption from the same gas. This distribution is far from an equilibrium distribution (see e.g. Nicastro et al. 1998), not an impossible situation considering the large variability observed in this source.

The absorption features seen between 1 and 2 keV may also be interpreted in terms of resonant lines (e.g. Leighly et al. 1997). If the ion producing the absorption is oxygen O VIII (resonant line at 0.65 keV), the best-fitting notch energy of 1.22 keV (quasar frame) implies a very high gas velocity: $-0.56c$. Fe XVIII ($E = 0.87$ keV) or Fe XVII ($E = 0.81$ keV) can also contribute to the absorption, because of their high oscillator strengths, 1.7 and 0.6 respectively (Kato 1976), and abundances. If the 1.22-keV absorption notch is caused by these ions, then the velocity of the outflowing gas will be smaller, $-0.33c$.

In any case, in the blueshifted absorption scenario the gas is outflowing at velocities that are a sizeable fraction of c, reminiscent of blobs of gas in jets. It is interesting to note that similar absorption features have been observed in blazars (e.g. PKS 2155 − 304, Canizares & Kruper 1984; other BlLacertae, Madejsky et al. 1991; and 3C 273, Grandi et al. 1997), but usually below 1 keV. Somewhat surprisingly this implies less extreme conditions in these radio-loud objects than in our radio-quiet quasars. High-redshift radio-loud quasars may have similar jet-related absorption too (Elvis et al. 1997).

An alternative interpretation of the 1-keV feature is in terms of an emission line due to highly ionized oxygen, neon (Ne IX) and/or to iron L. There are two possible origins for this line: recombination in an optically thin thermal plasma, or 'reflection' in photoionized matter.

5.2.1 *Thermal plasma*

A thermal plasma is highly implausible on physical grounds (Elvis et al. 1991; Fiore et al. 1995). Emission measure is $\sim 2.5 \times 10^{65}$ cm^{-3}. For a spherical source (with radius R) and constant electron density n_e, $n_e = 2.43 \times 10^{32} R^{-3/2}$ cm^{-3}. $R < 10^{14}$ cm from the observed X-ray variability, so $n_e < 1.5 \times 10^{12}$ cm^{-3}. This implies an electron scattering optical depth $\tau_T \gtrsim 30$. With such values a thermal plasma is no longer optically thin. The situation is even worse if the matter is clumpy, as the density of each cloud must be greater.

5.2.2 *Photoionized matter*

The second possibility is that the '1-keV' emitting matter is photoionized by the central nucleus. We can assume that the gas is not covering the source because there is no significant O VII and/or O VIII absorption. We therefore assume that we are not observing a 'warm absorber', but rather a 'warm reflector'. This could be either a warm absorber viewed from its side, in which case the matter would be optically thin to Thomson scattering; or the accretion disc, and the matter would be thick. Since both the 'reflector' and the primary emission (which provides most of the continuum) are observed, the optically thick case gives the highest values of the equivalent width (EW). However, even in the optically thick case, the expected EWs can barely account for the observed values (see below); hence we neglect the optically thin case altogether.

The observed line (which is significantly broad) may be a blend of several lines (see for instance Życki et al. 1994; Netzer 1996). The observed energy suggests the 0.92-keV Ne IX and 1.02-keV Ne X recombination lines, the 0.87-keV O VIII recombination (to ground state) line and the Fe L (around 0.8 keV) lines being the most important. None of these lines alone can account for the observed EW: for instance, the maximum value (i.e. for a face-on disc with an intervening ion fraction ~0.6) for the Ne IX line is about 10 eV, while that of the oxygen recombination line is about 15 eV (note that an O VIII Kα recombination line at 0.65 keV with a similar EW should also be present; the 90 per cent upper limit on such a line is

30 eV). These values have been calculated using the formulae of Basco (1978), and assuming a reasonable ionization structure. (In the disc hypothesis a Fe Kα line at 6.5–6.9 keV is also expected, but the upper limit of 300–400 eV does not exclude the presence of such a line.) Allowing for a possible factor of 2 neon and/or iron overabundance (an oxygen overabundance would decrease the Ne line while not increasing the O line) and/or anisotropy of the illuminating radiation, the observed equivalent width could be explained. (Note that in many Seyfert 1 galaxies the Fe Kα line is also stronger than expected, suggesting iron overabundance or anisotropic illumination.)

In this scenario the '1-keV' feature may arise from a highly ionized accretion disc. In the Matt et al. (1993) models, high ionization mainly arises because of high accretion rates (the ionization parameter depends on $\dot{m}^3$). The detection of these emission lines in steep soft X-ray quasars would then be further evidence of high $L/L_{\rm Edd}$. We note that, because recombination can occur only in highly ionized atoms, we would not expect features of this kind in 'normal' quasars, as their disc should be much less ionized, as in fact observed.

The strong dependence of the ionization parameter on $\dot{m}$ allows for large differences in the ionization structure against small differences in $\dot{m}$ and therefore that the '1-keV' feature may not be ubiquitous in NLSy1s. Indeed, a similar feature is not present in NAB 0205 + 024. A line with the same equivalent width as in PG 1244 + 026 (60 eV) would have been detected in the NAB 0205 + 024 SIS spectrum (the 90 per cent upper limit is only 20 eV). In the accretion disc scenario this would imply a different ionization state (higher or lower) of the matter or a significant metal underabundance in NAB 0205 + 024.

5.3 Variability

The mean 0.5–10 keV luminosity measured by *ASCA* in PG 1244 + 026 and NAB 0205 + 024 differs by an order of magnitude: 7.3×10^{43} and 6.4×10^{44} erg s^{-1} respectively (assuming isotropic emission, $H_0 = 50.0$ and $q_0 = 0.0$). The optical (3000 Å) monochromatic luminosities differ even more: 4×10^{43} and 9.4×10^{44} erg s^{-1} respectively. The variations seen in the NAB 0205 + 024 light curve imply an efficiency in the conversion of matter into radiation greater than 1.6 per cent (e.g. Fabian 1984). Taken at face value, this excludes thermonuclear reactions as the origin of the observed X-ray luminosity for which the upper limit on the efficiency is in this case about 0.7 per cent.

The similar variability observed in the two quasars agrees with the Fiore et al. (1998) finding that the variability properties of (PG) quasars are correlated with the shape of the soft X-ray spectrum and the width of the Balmer lines, and so possibly then with the accretion rate, in the scheme of Pounds et al. (1995) and Laor et al. (1994, 1997).

6 CONCLUSIONS

ASCA observations of two steep soft X-ray quasars have shown that:

(i) The X-ray continuum of the two quasars flattens by $\Delta\alpha = 0.5$–1 going towards high energies. Similar results were obtained by other authors on some half-dozen steep soft X-ray quasars.

(ii) PG 1244 + 026 shows a significant feature in the '1-keV' region. Similar features were again reported in other steep soft X-ray quasars. The data are not good enough to discriminate between a broad emission line centred at 0.95 keV (quasar frame) or an absorption edge at 1.17 keV, or an absorption notch at 1.22 keV. Line emission could be due to reflection from a highly ionized accretion disc, in line with the view that steep soft X-ray quasars are emitting close to the Eddington luminosity. Photoelectric edge absorption or resonant line absorption could be produced by gas outflowing at a large velocity (0.3–0.6 *c*). In these absorption models significant cold (i.e. oxygen less ionized than O VI) absorption in excess of the Galactic is required. This would imply an increase by a factor of 2–3 of the cold column with respect to a previous PSPC observation or a peculiar ionization structure. In neither the emission nor absorption cases is the SIS resolution good enough to identify unambiguously the ions responsible for the feature. The high resolution and high throughput of the low-energy gratings and spectrometers of *AXAF* and *XMM* are clearly needed to shed light on this puzzling case.

(iii) The two quasars show similar variability properties (flux variations up to a factor of 2 in 10 ks) despite a factor of 10 difference in the X-ray observed luminosity. This agrees with the Fiore et al. (1998) finding that the variability properties of radio-quiet quasars are correlated with the shape of the X-ray spectrum, the width of the Balmer lines and so possibly with the accretion rate.

ACKNOWLEDGMENTS

FF acknowledges support from NASA grants NAG 5-2476 and NAG 5-3039; BJW acknowledges support from ASC contract NAS8-39073.

REFERENCES

Barvainis R., 1993, ApJ, 412, 513
Basko M. M., 1978, ApJ, 223, 268
Boller Th., Brandt W. N., Fink H., 1996, A&A, 305, 53
Boller Th., Brandt W. N., Fabian A. C., Fink H., 1997, MNRAS, 289, 393
Brandt W. N., Fabian A. C., Nandra K., Reynolds C. S., Brinkmann W., 1994, MNRAS, 271, 958
Brandt W. N., Pounds K. A., Fink H. H., 1995, MNRAS, 273, 47
Brandt W. N., Mathur S., Elvis M., 1997, MNRAS, 285, L25
Canizares C. R., Kruper J., 1984, ApJL, 278, 99
Comastri A., Molendi S., Ulrich M.-H., 1995, in Makino F., Mitsuda K., eds, Proc. X-ray Imaging and Spectroscopy of Cosmic Hot Plasmas. Tokyo University Academy Press, Tokyo, p. 279
Comastri A. et al., 1998, A&A, in press
Czerny B., Elvis M., 1987, ApJ, 321, 305
Ebisawa K., 1991, PhD thesis, ISAS Research Note 483
Elvis M., Lockman F. J., Wilkes B. J., 1989, AJ, 97, 777
Elvis M., Giommi P., McDowell J., Wilkes B. J., 1991, ApJ, 378, 537
Elvis M. et al., 1994, ApJS, 95, 1
Elvis M., Fiore F., Giommi P., Padovani P., 1997, ApJ, 492, 91
Fabian A. C., 1984, Phys. Scr., T7, 129
Ferland G. J., 1996, CLOUDY 90.01
Fiore F., Elvis M., Mathur S., Wilkes B., McDowell J., 1993, ApJ, 415, 129
Fiore F., Elvis M., McDowell J. C., Siemiginowska A., Wilkes B. J., 1994, ApJ, 431, 515
Fiore F., Elvis M., Siemiginowska A., Wilkes B. J., McDowell J. C., Mathur S., 1995, ApJ, 449, 74
Fiore F., Matt G., Nicastro F., 1997, MNRAS, 284, 731
Fiore F., Laor A., Elvis M., Nicastro F., Giallongo E., 1998, ApJ, in press
Gehrels N., 1986, ApJ, 303, 336
Gendreau K., Yaqoob T., 1997, ASCA News, 5, 8
Grandi P. et al., 1997, A&A, 325, L17
Grupe D., 1996, PhD thesis, Univ. Göttingen
Kato T., 1976, ApJS, 30, 397

Laor A., Fiore F., Elvis E., Wilkes B. J., McDowell J. C., 1994, ApJ, 435, 611
Laor A., Fiore F., Elvis E., Wilkes B. J., McDowell J. C., 1997, ApJ, 477, 93
Lawrence A., Elvis M., Wilkes B. J., McHardy I., Brandt N., 1997, MNRAS, 285, 879
Leighly K. M., Mushotzky R., Nandra K., Forster K., 1997, ApJ, 489, L25
Madejsky G. M., Mushotzky R. F., Weaver K. A., Arnaud K. A., 191, ApJ, 370, 198
Matt G., Fabian A. C., Ross R. R., 1993, MNRAS, 264, 839
Mathur S., Wilkes B. J., Elvis M., Fiore F., 1994, ApJ, 434, 493
Nandra K., Pounds K. A., 1994, MNRAS, 268, 405
Nandra P., George I. M., Mushotzky R. F., Turner T. J., Yaqoob T., 1997, ApJ, 477, 602
Netzer H., 1996, ApJ, 473, 781
Nicastro F., Fiore F., Perola G. C., Elvis M., 1998, ApJ, submitted
Otani C., Kii T., Miya K., 1996, MPE Rep. 263, p. 491
Pounds K. A., Done C., Osborne J. P., 1995, MNRAS, 277, L5
Ptak A., Yaqoob T., Serlemitsos P. J., Mushotzky R., Otani C., 1994, ApJ, 436
Raymond J. C., Smith B. W., 1977, ApJS, 35, 419
Reynolds C. S., 1997, MNRAS, 287, 513
Tanaka Y., Inoue H., Holt S. S., 1994, PASJ, 46, L37
Turner T. J., Weaver K. A., Mushotzky R. F., Holt S. S., Madejsky G. M., 1991, ApJ, 381, 85
Walter R., Fink H., 1993, A&A, 274, 105
Życki P. T., Krolik J. H., Zdziarski A. A., Kallman T. R., 1994, ApJ, 437, 597

Reprinted from

PROCEEDINGS
SUPPLEMENTS
NUCLEAR PHYSICS B

Nuclear Physics B (Proc. Suppl.) 69/1–3 (1998) 501–504

A Resonant Absorption Line in the ASCA Spectrum of NGC 985?

F. Nicastro[a], F. Fiore[a] , N. Brandt[b] and C. S. Reynolds[c]

[a]Osservatorio Astronomico di Roma,
Via Osservatorio 2 - I00040 Monteporzio, Italy

[b]The Penn. State University; 525 Davey Lab,
University Park, PA 16802 USA

[c]JILA, University of Colorado,
Campus Box 440, Boulder CO 80309-0440, USA

ELSEVIER

ELSEVIER

Nuclear Physics B (Proc. Suppl.) 69/1-3 (1998) 501-504

NUCLEAR PHYSICS B
PROCEEDINGS
SUPPLEMENTS

A Resonant Absorption Line in the ASCA Spectrum of NGC 985?

F. Nicastro[a], F. Fiore[a] , N. Brandt[b] and C. S. Reynolds[c]

[a]Osservatorio Astronomico di Roma,
Via Osservatorio 2 - I00040 Monteporzio, Italy

[b]The Penn. State University; 525 Davey Lab,
University Park, PA 16802 USA

[c]JILA, University of Colorado,
Campus Box 440, Boulder CO 80309-0440, USA

We present timing and spectral analyses of the ASCA observation of the Seyfert 1 galaxy NGC 985. The 0.6-10 keV spectrum of this source is complex: large residuals are evident below 1 keV when fitting the spectrum with a power-law model. Fitting a warm absorber model to the 0.6-2.5 keV spectrum gives $\alpha = 1.12 \pm 0.04$, $\mathrm{Log}N_H^{WA} = 21.97 \pm 0.08$ and LogU$= 0.06 \pm 0.09$, but the residuals continue to show a deficit of counts between 0.9 and 1 keV. Adding an absorption line improves the fit, and the energy of the line is consistent with that of Kα NeIX-X resonant absorption lines. Hence, we confirm the presence of an ionized absorber along the line of sight to this source and interpret the further 1 keV spectral feature as the first detection of a strong resonant absorption line associated with this system. The extrapolation of this model above 2.5 keV produces large positive residuals above 3-4 keV. Fitting the data with a broken power law plus warm absorber model gives an acceptable χ^2 and $\Delta\alpha \sim 0.5$. A narrow iron line at 6.4 keV (quasar frame) of equivalent width 138^{+64}_{-110} eV is also present in the ASCA data.

1. Introduction

Absorption features from ionized gas are common in the X-ray spectra of type 1 AGN ([1]). Brandt et al. (1994, [2]) found a deep absorption edge in the ROSAT-PSPC spectrum of NGC 985, at an energy consistent with OVII-OVIII K edges.
Absorption K and L edges are not the only absorption features expected to be imprinted on X-ray spectra of warm absorbed sources. if the gas is not isotropically distributed around the ionizing source, resonant absorption lines should be present as well ([3]). Until now, none of the predicted resonant absorption lines have been clearly identified in the X-ray spectra of AGN known to host warm absorbers.

We present here the analysis of an ASCA observation of NGC 985. We confirm the presence of a warm absorber in this source. We also detect an additional absorption feature at 0.97 keV, which could be explained in terms of resonant scattering absorption from the warm gas.

2. Data Reduction and Analysis

NGC 985 was observed by ASCA on August 12, 1996 with a total exposure of ~ 40 ksec. SIS and GIS count rates were 0.25 counts s^{-1} and 0.18 counts s^{-1} respectively.

We applied standard screening procedures (following Reynolds 1997, [1]). We extracted source counts from regions of 4' and 6' radius for SIS and GIS respectively. Both local and blank-sky field backgrounds were tested. We did not find significant differences between the two cases. In the following we present the results obtained using the background from the blank fields.

2.1. Timing Analysis

The source intensity changes by a factor ~ 1.4 during the observation. Fig. 1 shows the SIS and GIS light curves. We grouped the data in bins of 500 s. Changes are more marked in the SIS light curve, suggesting spectral variability as-

PII S0920-5632(98)00270-9

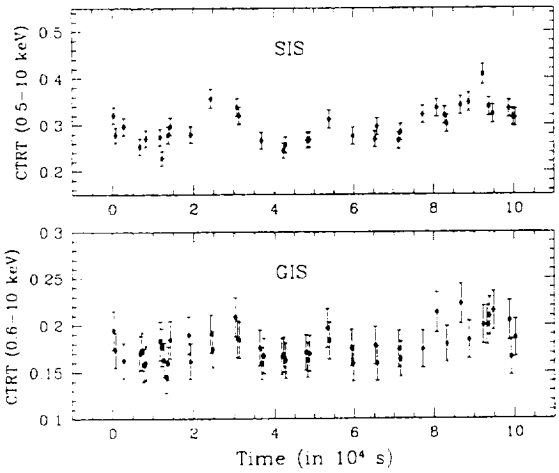

Figure 1. SIS and GIS light curves of the ASCA observation of NGC 985.

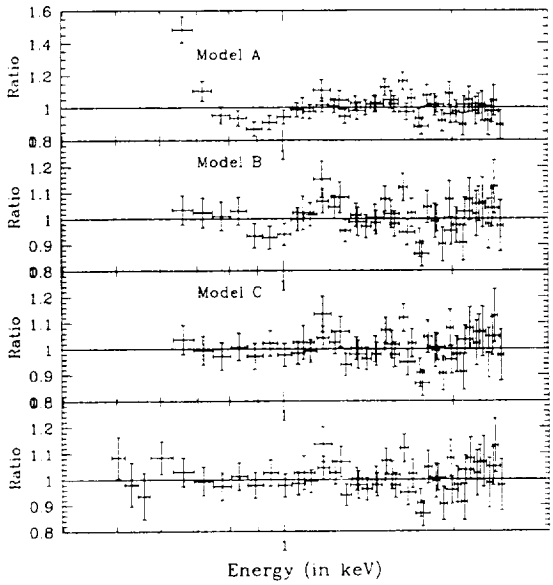

Figure 2. Residuals after fitting the 0.6–2.5 keV data with models A (upper panel), B (second panel) and C (third panel). The lower panel shows the residuals after the extrapolation of the 0.6–2.5 keV best fit Model C down to 0.45 keV.

sociated with the soft component. However the quality of the data and the small dynamical range of variability does not allow a detailed study of the spectral variability.

2.2. Spectral Analysis

We fitted the SIS spectra in the 0.6–8 keV energy band and the GIS spectra in the 1–10 keV band.

2.2.1. Soft (0.6–2.5 keV) X-ray Spectrum

Table 1 shows the results of the fits to the 0.6–2.5 keV SIS and GIS spectra. In Fig. 2 we show the ratio between data and best fit models. We first fitted the spectra with a simple power law, reduced at low energy by cold absorption (Model A). This fit is unacceptable and the absorption is not consistent with the Galactic value along the line of sight (3.0×10^{20} cm^{-2}). Large positive and negative residuals are evident below $\sim$ 1 keV in the upper panel of Fig. 2, suggesting the presence of either a soft excess, a warm absorber component, or both. A warm absorber component associated with NGC 985 has already been proposed by Brandt et al. (1994, [2]) in their analysis of ROSAT data of this source. We therefore added a photoionization model (built with CLOUDY, ver. 90.01, [4]) to Model A, and refitted the data fixing N_H to the Galactic value (Model B). Power-law index, U and N_H^{WA} were left free to vary. Residuals to the best fit model are shown in the second panel of Fig. 2: a deficit of counts is still evident between 0.9 and 1 keV.

We then added a negative Gaussian to the previous model, and refitted the data (Model C). The addition of this component provides a highly significant improvement in χ^2: F(2,40) = 11.6, corresponding to a probability of $< 1\%$. Residuals to this model are shown in the third panel of Fig. 2. The best fit continuum and warm absorber parameters are quite similar to those obtained fitting the data without the absorption line. The best fit line energy is $0.97^{+0.04}_{-0.05}$, consistent with a blend of NeIX–X Kα resonant absorption lines (at the source redshift of 0.043). The equivalent width is $18.7^{+9.6}_{-8.7}$ eV.

2.2.2. 0.6–10 keV X-ray Spectrum

Fig. 3 shows the residuals from the extrapolation of the best fit Model C up to 10 keV. A clear flattening of the spectrum is present above 3 keV.

Table 1
Spectral fits to the 0.6–2.5 keV SIS+GIS spectra

Model	$^{a}N_H$	α	^{b}norm.	$^{c}\mathrm{Log}N_H^{WA}$	LogU
	$^{d}\mathrm{E}_{line}^{abs}$	$^{e}\mathrm{EW}^{abs}$	χ^2_τ(dof)		
A	< 0.9	0.31 ± 0.06	$1.55^{+0.07}_{-0.03}$		–
	–	–	2.31(42)		
B	3.02(fix)	1.12 ± 0.04	$3.50^{+0.08}_{-0.05}$	21.97 ± 0.08	0.06 ± 0.09
	–	–	1.24(40)		
C	3.02(fix)	1.08 ± 0.04	$3.32^{+0.07}_{-0.06}$	21.92 ± 0.09	0.07 ± 0.09
	$0.97^{+0.04}_{-0.05}$	$18.7^{+9.6}_{-8.7}$	1.0(38)		

[a] In 10^{20} cm^{-2}. [b] In 10^{-3} ph cm^{-2} s^{-1} keV^{-1}, at 1 keV. [c] In Log(cm^{-2}). [d] In keV. [e] In eV.

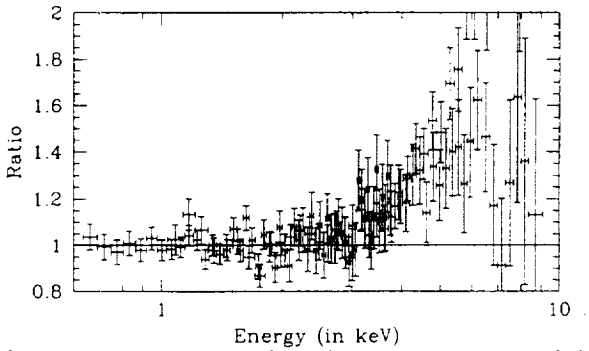

Figure 3. Residuals after the extrapolation of the best fit Model C up to 10 keV. A clear flattening of the spectrum is present above 2–3 keV.

We then repeated the fit substituting in Model C the simple power law with a broken power law, fixing the low energy spectral index to the best fit value of Model C, and allowing the break energy and the hard spectral index to vary (Model D). Results are presented in Table 2.
Finally we added a narrow line at 6.4 keV (quasar frame), to Model D, and refitted the data (Model E: table 2). The addition of the iron line to Model D is significant: F(1,108)=7, corresponding to P$\sim$1%. The equivalent width is 138^{+64}_{-110} eV.

3. Physical Interpretation of the 1 keV spectral feature

A number of possible interpretations could be invoked to explain the 1 keV absorption feature present in the ASCA spectrum of NGC 985. These include non-equilibrium effects, which would produce emerging spectra quite different from those expected at equilibrium ([5]), multi-zone geometrical configurations, in which a number of clouds of gas with different column densities and ionization states would obscure the line of sight and imprint different absorption features in the emerging spectrum ([6]), or continuum effects. Another possible explanation is provided by resonance absorption lines in the context of a simple single-zone, equilibrium photoionizaion model ([7]). In the following we discuss this latter possibility. A complete presentation of all the above possibilities is deferred to a forthcoming paper.

Resonant absorption lines are expected in the X-ray spectra emerging from ionized gas. Many of these atomic transitions have negligible oscillator strengths, and/or are produced by elements with low cosmic abundance. In a few cases (Kα resonant lines of C, O, Ne and Fe, and L iron lines), the lines are particularly intense (equivalent widths $\gtrsim$ 20 eV for turbulence velocity $\gtrsim$ 100 km/s) and have energies between 0.1 and 10 keV. We have built a simple code to calculate the equivalent width (and so the growth curves) and the profile of the main resonant absorption lines of C, O, Ne and Fe. The intensities of these lines depend on the geometrical configuration and distribution of the gas around the central source. We run our program using the best fit N_H and U values of Model C, and assuming a simple geometrical configuration: a single cloud obscuring our line of sight. Fig. 4 shows the spectra (rest frame)

Table 2
Spectral fits to the 0.6–10 keV SIS+GIS spectra

Model	E_b	α_H	[a]norm.	[b]EW^{em}	χ^2_r(dof)
D	2.75 ± 0.25	0.51 ± 0.06	3.35 ± 0.05	-	0.95(108)
E	2.66 ± 0.25	0.56 ± 0.05	3.35 ± 0.05	138^{+64}_{-110}	0.90(107)

[a] In 10^{-3} ph cm^{-2} s^{-1} keV^{-1}, at 1 keV. [b] In eV.
note: We list only the parameters left free to vary in the fit. Other parameters are fixed to the best fit value of Model C. The emission line energy is fixed to 6.4 keV (source frame).

transmitted from such a cloud of ionized gas (the edge-like absorption features are those predicted by CLOUDY), for turbulence velocities of 100 km/s (left panel) and 1000 km/s (right panel) respectively. The dashed line at 0.6 keV shows the lower end of the SIS band. OVII and OVIII absorption K edges are clearly visible in the spectra, along with the strong Kα resonant absorption lines of NeIX and NeX. The total predicted equivalent width of the NeIX–X lines ranges from 5 eV to 20 eV, for turbulence velocities between 100 and 1000 km/s. OVII and OVIII $K\alpha$ resonant absorption lines are also present in the spectra of Fig. 4, with total equivalent widths of 5.5 eV (left panel) and 30 eV (right panel). They lie at the lower end of the considered SIS energy range. However residuals after the extrapolation of the 0.6–2.5 keV best fit Model C down to 0.45 keV show an absorption-like feature (Fig. 2, lower panel). The uncertain SIS calibration below 0.6 keV does not allow us to draw a definitive conclusion.

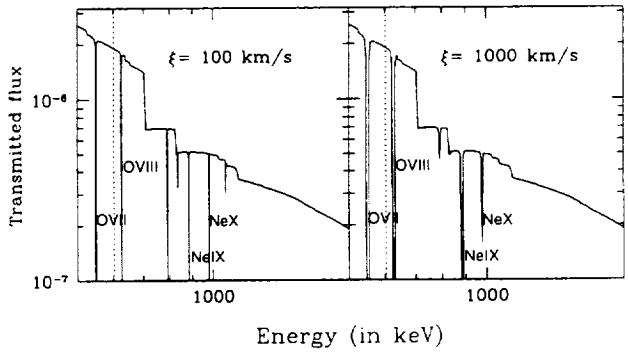

Figure 4. Spectra (in the observer frame) transmitted from a cloud of ionized gas with N_H and U from the best fit values of Model C, for turbulence velocities of 100 km/s (left panel) and 1000 km/s (right panel) respectively.

4. Conclusion

We present timing and spectral analyses of the ASCA data of the Seyfert 1 galaxy NGC 985, and find the following main results: (a) we confirm the presence of a warm absorber along the line of sight of NGC 985; (b) we detect an additional absorption feature at 0.97 keV (rest frame); (c) we interpret this feature as due to a blend of NeIX and NeX Kα resonant absorption lines from the ionized gas; (d) the spectrum of NGC 985 flattens above 3 keV by $\Delta\alpha = 0.5$; (e) a narrow emission line at 6.4 keV (quasar frame) is also seen in the data, with an equivalent width of 138 eV.

Aknowledgements: C.S.R. thanks the National Science Foundation for support under grant AST-9529175, and NASA for support under grant NASA-NAG-6337. F.F. acknowledges support from NASA grant NAG5-2476.

REFERENCES

1. C. Reynolds, 1997, M.N.R.A.S., 286, 513
2. N. Brandt et al., M.N.R.A.S., 271, 958
3. Y. Ueda et al., 1997, in press
4. G.J. Ferland, 1996, CLOUDY, ver. 90.01
5. F. Nicastro, F. Fiore, G. C. Perola and M. Elvis, 1997, submitted to Ap.J.
6. G.A. Kriss et al., 1996, Ap.J. 467, 629
7. F. NIcastro, F. Fiore and G. Matt, Ap.J., in preparation

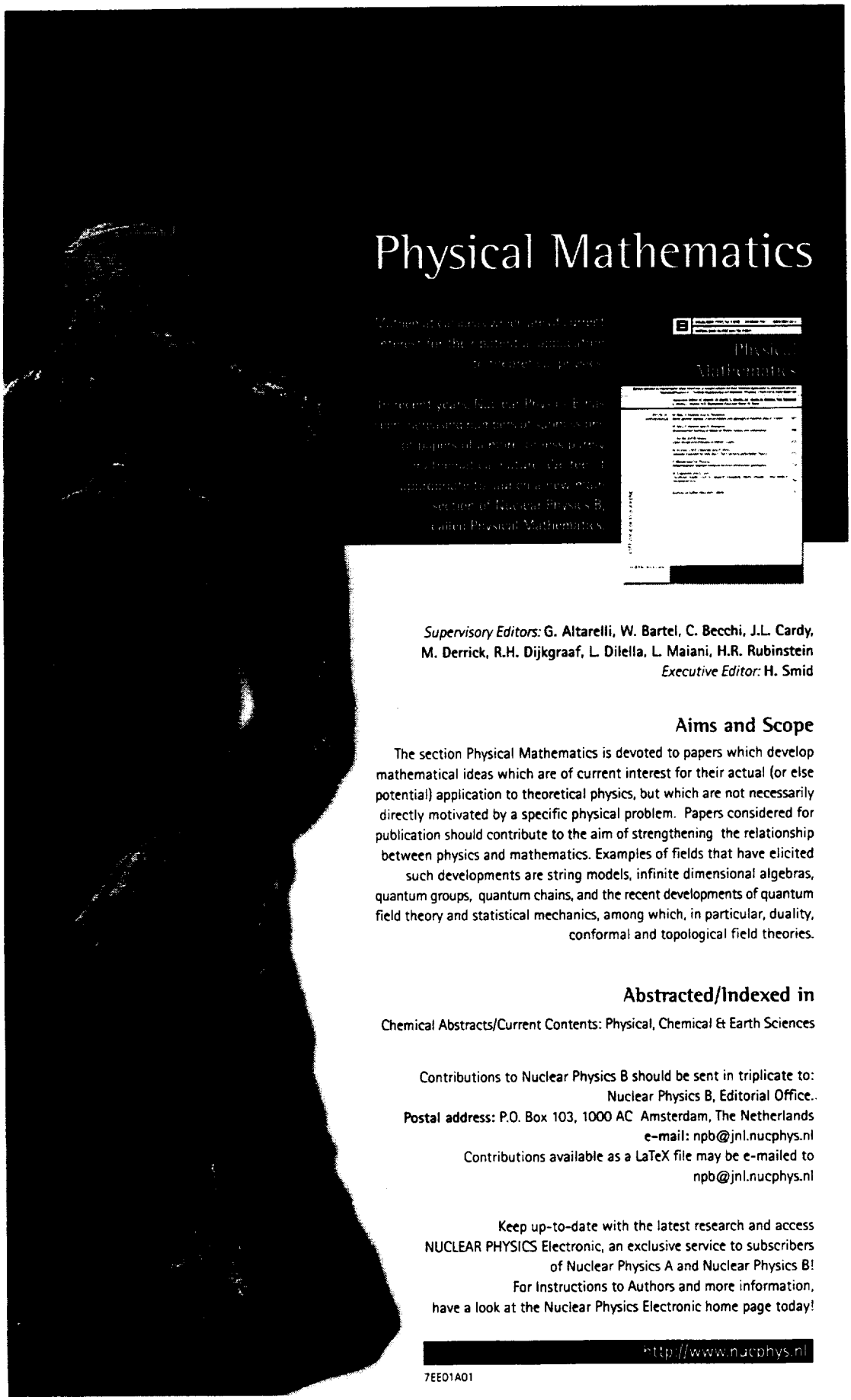

Aims and Scope

The section Physical Mathematics is devoted to papers which develop mathematical ideas which are of current interest for their actual (or else potential) application to theoretical physics, but which are not necessarily directly motivated by a specific physical problem. Papers considered for publication should contribute to the aim of strengthening the relationship between physics and mathematics. Examples of fields that have elicited such developments are string models, infinite dimensional algebras, quantum groups, quantum chains, and the recent developments of quantum field theory and statistical mechanics, among which, in particular, duality, conformal and topological field theories.

Abstracted/Indexed in

Chemical Abstracts/Current Contents: Physical, Chemical & Earth Sciences

Contributions to Nuclear Physics B should be sent in triplicate to:
Nuclear Physics B, Editorial Office..
Postal address: P.O. Box 103, 1000 AC Amsterdam, The Netherlands
e-mail: npb@jnl.nucphys.nl
Contributions available as a LaTeX file may be e-mailed to
npb@jnl.nucphys.nl

THE ASTROPHYSICAL JOURNAL, 517:108–122, 1999 May 20

RESONANT ABSORPTION IN THE ACTIVE GALACTIC NUCLEUS SPECTRA EMERGING FROM PHOTOIONIZED GAS: DIFFERENCES BETWEEN STEEP AND FLAT IONIZING CONTINUA

FABRIZIO NICASTRO,[1,2,3] FABRIZIO FIORE,[1,2,4] AND GIORGIO MATT[5]
Received 1998 September 8; accepted 1998 December 29

ABSTRACT

We present photoionization models accounting for both photoelectric and resonant absorption. Resonance absorption lines from C, O, Ne, Mg, Si, S, and Fe between 0.1 and 10 keV are treated. In particular we consider the complex of almost 60 strong Fe L absorption lines around 1 keV. We calculate profiles, intensities, and equivalent widths of each line, considering both Doppler and natural broadening mechanisms. Doppler broadening includes a term accounting for turbulence of the gas along the line of sight. We computed spectra transmitted by gas illuminated by drastically different ionizing continua and compared them to spectra observed in flat X-ray spectrum, broad optical emission-line type 1 active galactic nuclei (AGNs), and steep X-ray spectrum, narrow optical emission-line type 1 AGNs. We show that the ~ 1 keV absorption feature observed in moderate-resolution X-ray spectra of several narrow-line Seyfert 1 galaxies can be explained by photoionization models, taking into account resonance absorption, without requiring relativistic outflowing velocities of the gas, if the physical properties of these absorbers are close to those found in flat X-ray spectrum Seyfert 1 galaxies. We finally present simulations of the spectra emerging from gas illuminated by both steep and flat ionizing continua, as seen by the *AXAF* high-energy transmission gratings and the baseline Constellation-X calorimeter. We discuss briefly the relevant physics that can be investigated with these instruments.

Subject headings: galaxies: active — galaxies: Seyfert — line: formation — radiative transfer — X-rays: galaxies

1. INTRODUCTION

The *ROSAT* (Trümper 1983) PSPC (Pfefferman et al. 1987) has found a large spread in the spectral indices of type 1 active galactic nuclei (AGNs): $0.5 < \alpha_E < 3$ [$f(E) = E^{-\alpha_E}$; Laor et al. 1997; Walter & Fink 1993; Fiore et al. 1994]. This remarkably broad soft X-ray spectral index distribution appears not to be random, but rather strongly correlated with other important optical and X-ray properties of these objects. Objects with narrower Hβ ($1000 < \mathrm{FWHM} < 2000$ km s^{-1}) and smaller [O III]/Hβ(< 1) ratio are systematically steeper in soft X-rays ($\alpha_E > 1.5$) than AGNs with broad (FWHM > 2000 km s^{-1}) permitted lines and greater [O III]/Hβ ratio ($1 <$ [O III]/H$\beta < 3$, $\alpha_{\mathrm{PSPC}} < 1.5$). In particular most of the so-called narrow-line Seyfert 1 galaxies (NLSy1s) show a steep 0.2–2 keV continuum (Boller, Brandt, & Fink 1996). In the 2–10 keV energy range narrow optical emission-line quasars have still a somewhat steeper spectrum compared to broad optical emission-line quasars. The spread of the 2–10 keV spectral index is, however, smaller than that of the 0.1–2 keV PSPC one (Brandt, Mathur, & Elvis 1997). It has been suggested that these properties are correlated with the accretion rate (Pounds, Done, & Osborne 1995; Laor et al. 1997; Fiore et al. 1998a, 1998b).

Ionized gas, modifying the AGN X-ray spectrum, has been detected in about half of the bright, X-ray flat, broad optical emission-line type 1 AGNs studied by *ASCA* (Reynolds 1997; George et al. 1998). The main features imprinted by the ionized gas on the X-ray spectrum are the O VII and O VIII K absorption edges at 0.74 and 0.87 keV. As already pointed out by George et al. (1998), the similarity of the parameters of these features among different sources in both the Reynolds (1997) and the George et al. (1998) samples implies that "warm" absorbers in AGNs all have roughly similar ionization structure, despite the broad range of ionizing luminosity (i.e., about 3 orders of magnitude, from $\sim 10^{41}$ to 10^{44} ergs s^{-1}). In terms of the ionization parameter U, the presence in the gas of He-like and H-like ions of C, O, and Ne as dominant ionic species implies a narrow range of $\log U = 0.5$–1.5 (Nicastro et al. 1999). This is consistent with the location of the warm gas at radii scaling with the square root of the luminosity. The column densities of the Reynolds sample are distributed in the range $\log N_{\mathrm{H}} = 21$–23, but the standard deviation of the distribution is rather small, $\sigma_{\log N_{\mathrm{H}}} = 0.3$, again indicating a relative uniformity in the physical properties of this AGN component. Several type 1 AGNs showing ionized absorption features in X-ray also show high-ionization UV absorption lines (namely, O VI, N V, C IV, C III]), superposed to the broad emission lines and systematically blueshifted with respect to them (Mathur et al. 1994; Mathur, Elvis, & Wilkes 1995; Mathur, Wilkes, & Elvis 1998). The widths of these absorption lines are typically much broader than the associated thermal broadening, suggesting turbulence velocities of the absorber. The UV and the X-ray absorbers have ionization states compatible with each other, which supports the identification of these two components (Mathur et al. 1994, 1995, 1998; Mathur, Wilkes, & Aldcroft 1997). In one of these cases (the Seyfert 1 galaxy NGC 3516) the total column density implied by some strong UV absorption lines is larger than that required by the X-ray absorption features (Kriss et al. 1996a, 1996b). However it is

[1] Harvard-Smithsonian Center for Astrophysics, 60 Garden Street, Cambridge, MA 02138.
[2] Osservatorio Astronomico di Roma, via Osservatorio, Monteporzio-Catone (RM), I00040 Italy.
[3] Istituto di Astrofisica Spaziale—CNR, Via del Fosso del Cavaliere, Roma, I-00133 Italy.
[4] *BeppoSAX* Science Data Center, via Corcolle 19, Roma I00100 Italy.
[5] Dipartimento di Fisica, Università degli Studi "Roma Tre" Via della Vasca Navale 84, Roma, I00146 Italy.

quite possible that more than one kinematic component contributes to the total intensity and equivalent width of the UV lines and that only one of those is physically associated with the X-ray absorber (Mathur et al. 1997). The UV absorption lines may be produced in a turbulent outflowing wind intercepting the line of sight (possibly driven out by radiative acceleration). The outflowing velocities of the UV warm gas span the range $v_{out} \sim 100$–2000 km s^{-1} (Mathur et al. 1994, 1995, 1997), and a similar range has been estimated for the dispersion velocities σ_v along the line of sight.

On the other hand, deep absorption features at the energies of the K edges of highly ionized oxygen have never been observed in the 0.1–2 keV spectra of soft X-ray steep spectrum, narrow optical emission-line type 1 AGNs. Detections of deep oxygen edges have been reported for two sources previously classified as NLSy1 (IRAS 17020+4544, Leighly et al. 1997; Mrk 766, Matt et al. 1999). During the *ASCA* (0.5–10 keV) and *BeppoSAX* (0.1–10 keV) observations the two sources have a rather flat X-ray continuum ($\alpha_E \sim 1$) and therefore cannot be considered X-ray steep AGNs. Large variations of the X-ray spectral shape have already been observed in the past (e.g., 1H 0419−577, Guainazzi et al. 1999, Turner et al. 1999; NGC 4051, Guainazzi et al. 1998; RE J2248−511, Puchnarewicz et al. 1995). It is quite possible that a population of (perhaps low mass) AGNs does exist, switching between soft, high states and hard, low states (depending possibly on the accretion rate), and therefore classified in one way or in the other depending on the observed state (in analogy to what is seen in Galactic black hole candidates).

Despite the lack of oxygen edges, steep soft X-ray spectrum, narrow optical emission-line, type 1 AGNs are usually far from being featureless (Brandt 1995; Hayashida 1997). *ASCA* has found large residuals between 1 and 2 keV, after subtracting the appropriate continuum, in at least four cases (Leighly et al. 1997; Fiore et al. 1998b). The interpretation of these features is not unique, given the relatively modest spectral resolution of the *ASCA* SIS and the complexity of the continua. Leighly et al. (1997) interpret the features found in the three NLSy1s studied in terms of O VII and O VIII resonance absorption lines blushifted by $\sim 0.5c$. Fiore et al. (1998b) interpret the feature found in PG 1244+026 in terms of either an emission line at 0.92 keV or Fe XVIII and Fe XVII resonant absorption blueshifted by $\sim 0.3c$.

Photoionization models used to fit and interpret AGN spectra usually deal with photoelectric absorption only. Matt (1994) and Krolik & Kriss (1995) were the first to point out the importance of X-ray resonant absorption lines in ionized absorbers. Here we calculate in detail photoionization models, including all the relevant resonant absorption lines, and study the dependence of the transmitted spectrum on the exact shape of the ionizing continuum. We find that the phenomenologies observed in both broad optical emission-line type 1 AGNs and NLSy1 galaxies can be explained in terms of their quite different ionizing continua, provided that, for a given luminosity, the radial distance of the gas clouds from the ionizing source (in units of gravitational radii) and the gas density are similar in both classes of objects.

Netzer (1993, 1996) discussed the relevance of recombination and fluorescent emission lines, provided that the covering factor of the ionized matter is significant, whereas Krolik & Kriss (1995) and Matt, Brandt, & Fabian (1996) pointed out that resonant scattering lines can be even more intense. Here, for the sake of simplicity, we do not consider any line emission, and therefore our model is strictly valid only if the covering factor is negligible (see next section).

In § 2 we present our photoelectric plus resonant absorption model and discuss the relevant physics. Section 2.3 compares the transmitted spectra computed with our models for two different ionizing continua with the spectra of a broad optical emission-line type 1 AGNs and a NLSy1 galaxy actually observed by *ASCA* ($\Delta E = 100$ eV, effective area ~ 500 cm^2). Section 3 presents a set of simulations with instruments of much higher spectral resolution (*AXAF* high-energy transmission gratings [HETG] $\Delta E = 1.5$ eV, collecting area ~ 100 cm^2, *AXAF* Proposer's Guide version 1.0, 1997[6]; and Constellation-X baseline calorimeter, $\Delta E = 3$ eV, collecting area $\sim 10{,}000$ cm^2, The High Throughput X-Ray Spectroscopy [HTXS] Mission, 1997[7]). We finally present our conclusions in § 4.

2. MODELS

We calculated the curves of growth of all the 268 permitted resonant absorption lines of C, O, Ne, Mg, Si, S, and Fe in the 0.1–10 keV energy range with oscillator strengths greater than 0.05. We used atomic data from the complete list of permitted LS-type (LS coupling transitions) resonant lines of all ionization states of 18 elements tabulated in Verner, Verner, & Ferland (1996). Intercombination and forbidden lines are not included in that compilation. We carried out the calculations considering the exact Voigt profile for the lines, i.e., considering both Doppler and natural broadening. As suggested by the width of the absorption lines detected in the UV spectra of the UV/X-ray ionized absorbers (Mathur et al. 1994, 1995, 1997, 1998), in addition to the thermal Doppler broadening we consider here a term accounting for gas turbulence and refer to this term as the "turbulence velocity" σ_v along the line of sight.

We calculated spectra emerging from photoionized gas for a number of values of N_H, U, and σ_v. Relative ionic abundances and edge-like absorption features for given U and N_H and for a particular shape of the nuclear ionizing continuum are those calculated by CLOUDY (Ferland 1997, version 90.04), whereas the intensity and profile of the resonance absorption lines are consistently computed here for a given value of σ_v. The result is an emerging spectrum including both absorption edges and lines.

We considered only line absorption, not emission. We used CLOUDY (version 90.04, Ferland 1997) to build total (transmitted plus emitted) spectra and verified that, for the range of total column densities and ionization parameters considered here, this assumption corresponds (for a spherical configuration) to covering factors $f_c < 0.1$ (in good agreement with the Netzer 1993 results; see his Fig. 3). In an ideal optically thin case in which (1) the ionized gas isotropically and uniformly covers the central source ($f_c = 1$), (2) any systematic (inflowing or outflowing) motion of the gas is absent, and (3) any line destruction mechanism (autoionization, Compton scattering, photoabsorption) is inefficient, then scattering of the resonant emission-line photons in the line of sight would exactly compensate for the line absorption along the line of sight, and, according to

[6] http://asc.harvard.edu/udocs/docs/PG_frame.html.
[7] http://constellation.gsfc.nasa.gov/documentation.html.

Netzer (1996), only emission features (mainly recombination lines) would be present in the total spectra. Any deviation from the above ideal condition would produce net absorption lines, which can therefore diagnose the physical and geometrical conditions of the absorbing material. Presence of outflows instead would imply that both emission and absorption lines are present in the emergent spectra, with the absorption lines blueshifted with respect to the emission ones. In this paper, however, for the sake of simplicity we assume that a cloud of gas with negligible covering factor ($f_c < 0.1$) is completely obscuring the line of sight, and therefore that the contribution from emission lines to the overall spectrum is negligible. In comparing our model with real spectra it must be kept in mind that absorption lines may be partly compensated by line scattering and recombination lines for significant covering factors or that emission lines may appear redward (blueward) of the absorption lines if the matter is outflowing (inflowing).

In the next section we present the details of the computation and show some examples of both growth curves and emerging spectra.

2.1. *Computation*

The equivalent width of a resonant absorption line is

$$\mathrm{EW} = \int_0^{+\infty} (1 - e^{-\tau_\nu}) d\nu \,, \tag{1}$$

where τ_ν is the dimensionless specific optical depth of the considered transition

$$\tau_\nu = \int_0^L ds \alpha_\nu = n_l L \frac{\pi e^2}{mc} f_{\mathrm{lu}} \Phi(\nu) \,. \tag{2}$$

In the above equation α_ν is the absorption coefficient at the frequency ν in cm^{-1}, n_l is the number density of ions of the given element that populates the lower level in the unit volume (in cm^{-3}), L is the linear dimension of the cloud of gas along the line of sight (in centimeters), f_{lu} is the oscillator strength of the electron transition from the lower to the upper level, m is the electron mass in grams, and $\Phi(\nu)$ is the normalized Voigt profile. With these units the equivalent width in equation (1) is in hertz. The Voigt profile can be written as (e.g., Rybicky & Lightman 1979)

$$\Phi(\nu) = \frac{1}{\sqrt{\pi} \Delta\nu_D} H(a, u) \,, \tag{3}$$

where $H(a, u)$ is the Voigt function:

$$H(a, u) = \frac{a}{\pi} \int_{-\infty}^{+\infty} \frac{e^{-y^2} dy}{a^2 + (u - y)^2} \,. \tag{4}$$

In equation (4) a is essentially the ratio between the natural and the Doppler line widths Γ and $\Delta\nu_D$, and $u = (\nu - \nu_0)/\Delta\nu_D$. For small values of a the center of the line is dominated by the Doppler profile, whereas the wings are dominated by the Lorentzian profile. As is well known, this influences the growth curves, making them increase with N_{H} even over the core saturation.

We consider two different contributions to the Doppler profile: (1) the thermal motion of the ions and (2) the dispersion velocity σ_v of the gas along the line of sight:

$$\Delta\nu_D = \frac{\nu_0}{c} \left(\frac{2kT}{M} + \sigma_v^2 \right)^{0.5} \,. \tag{5}$$

Let us estimate the relative contribution of the two terms in equation (5):

$$\frac{v^{\mathrm{therm}}}{\sigma_v} = \frac{\sqrt{2kT}}{\sqrt{m}\,\sigma_v} \simeq 1.3 \frac{(T)_6^{0.5} A^{-0.5}}{(\sigma_v)_{100}} \,. \tag{6}$$

In equation (6) $(T)_6$ is the equilibrium temperature of the gas in units of 10^6 K, $(\sigma_v)_{100}$ is the dispersion velocity in units of 100 km s^{-1}, and A is the atomic weight of the considered element. For a highly ionized gas in photoionization equilibrium, the temperature spans the range $(T)_6 \sim 0.1$–1. In such a gas the elements lighter than O-Ne are usually fully stripped (the threshold element over which bound ions are still present depending strongly on the photoionizing continuum shape), and so the residual opacity from both bound-free and bound-bound transitions is mainly due to the heavy elements (from O to Fe). Assuming therefore $(T)_6 = 0.5$, $(\sigma_v)_{100} = 1$, and $A = 16$ (the atomic weight of the lightest non–fully stripped element), we get, from equation (6), $v^{\mathrm{therm}}/\sigma_v \simeq 0.2$. For the iron ions ($A = 56$) we would find $v^{\mathrm{therm}}/\sigma_v \simeq 0.1$. Hence, for dispersion velocities of ~ 100 km s^{-1}, the contribution of the thermal motion of the ions to the broadening of the absorption line is only $\sim 10\%$–20% of the total, and it decreases linearly with increasing σ_v. Therefore, the second term in equation (5) is the dominant one for $(\sigma_v)_{100} \gtrsim 1$.

2.2. *Growth Curves*

Figures 1 and 2 show the growth curves of the Kα and Kβ lines of H-like and He-like C, O, Ne, and Fe, for (1) $\sigma_v = 0$ (Doppler broadening entirely due to the thermal motion of the ions), and (2) $\sigma_v = 1000$ km s^{-1}, respectively. The equivalent widths of the two Kα lines of H-like ions have been summed to give a single equivalent width for the doublet.

The ionization state of the absorbing gas is that of a typical flat X-ray spectrum, broad optical emission-line type 1 AGN "warm absorber" (log $U = 1$) for C, O, and Ne, whereas a much higher ionization case (log $U = 3$) is adopted for the Fe XXV and Fe XXVI lines. In both cases the ionizing continuum used is the AGN spectral energy distribution (SED), tabulated in CLOUDY (Ferland 1997, version 90.04). However, we stress that the growth curves depend only on the relative abundance of the ion under investigation and not on the particular combination of U and shape of the ionizing continuum producing this abundance.

At low column densities ($\lesssim 10^{21}$–10^{23} cm^2, the exact value depending on the considered line and dispersion velocity), the equivalent width of each line increases linearly with N_{H}. For higher values of N_{H} the optical depth of the line core saturates and the Lorentzian profile begins to drive the further slower growth of the equivalent width with increasing columns. The linear branch of the growth curves (the low column density limit) is described by equation (1) in the limit $\tau_\nu \ll 1$:

$$\mathrm{EW} \simeq \int_0^{+\infty} d\nu \tau_\nu = n_l L \frac{\pi e^2}{mc} f_{\mathrm{lu}} = \tau_{\mathrm{tot}} \,. \tag{7}$$

Let us define A_{X}, $\xi_{\mathrm{X}i}$, and N_{H} as the abundance of the element X relative to the H abundance, the relative abundance of the ion i of the element X, and the equivalent hydrogen column density along the line of sight, respectively. With these positions and introducing an appropriate

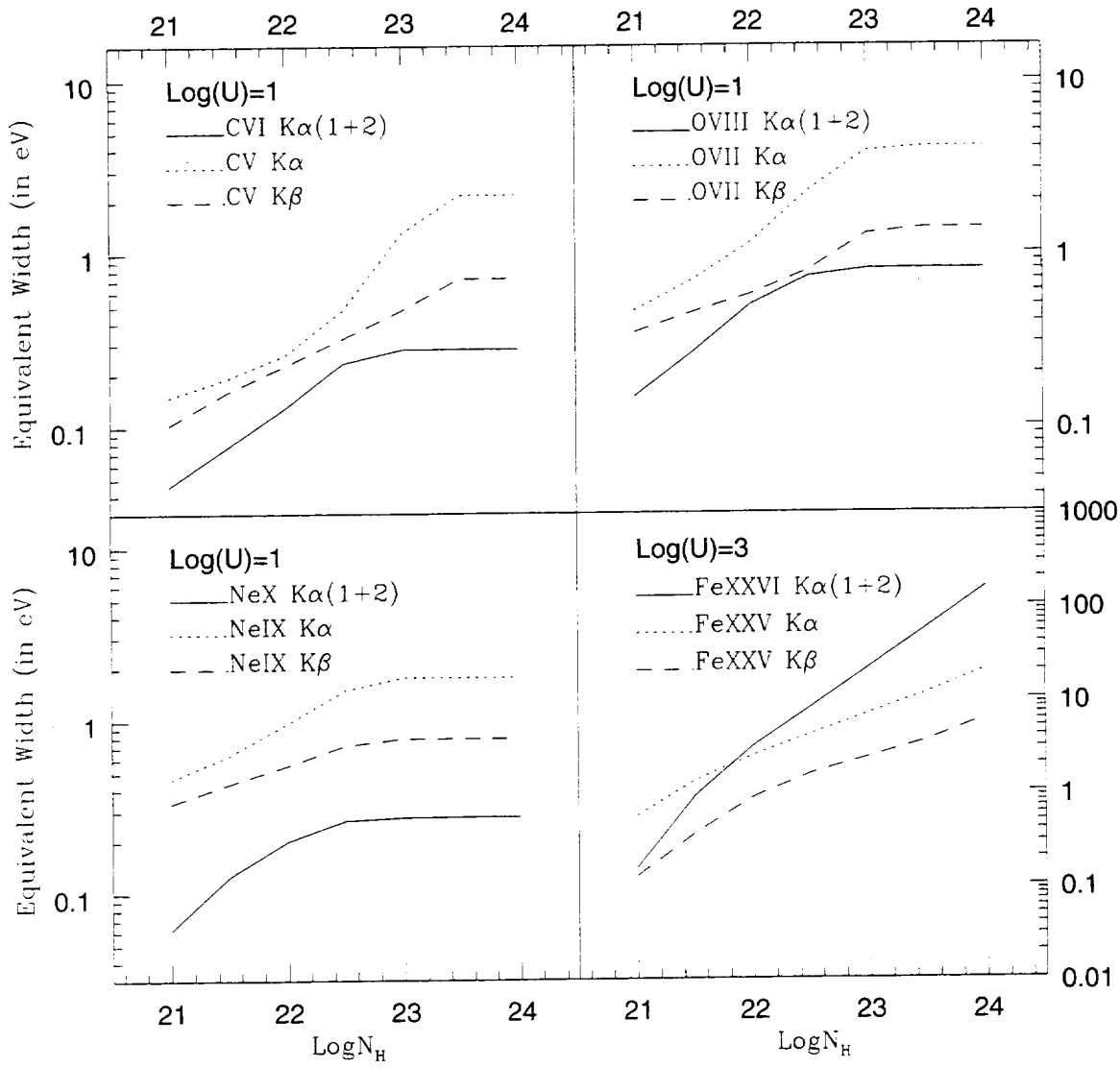

FIG. 1.—Growth curves of the Kα and Kβ lines of H-like and He-like C, O, Ne, and Fe, for $\sigma_v = 0$. The ionization state of the absorbing gas is that of a typical warm absorber (log $U = 1$) for C, O, and Ne and a much higher ionization case (log $U = 3$) for Fe XXV and Fe XXVI.

numerical format we have

$$\mathrm{EW} \simeq 2.2(\xi_{\mathrm{X}i})_{0.4}(A_{\mathrm{X}})_{-5}(\mathrm{N})_{22}(f_{\mathrm{lu}})_{0.5}\ \mathrm{eV}\ . \tag{8}$$

When the core of the line becomes opaque to the radiation, equation (8) is no longer valid, and the computation of the equivalent width must be carried out using equation (1) with the exact shape of the profile function. A comparison between the curves in Figure 1 and those in Figure 2 allows evaluation of the effects of the line profile upon the resulting equivalent width. When the Doppler broadening is dominated by the thermal motion of the ions ($\sigma_v \ll 100$ km s^{-1}, Fig. 1), the dynamical range of variation of the equivalent width of each line with increasing N_{H} is much smaller than in the case in which the Doppler broadening is dominated by a high dispersion velocity of the gas along the line of sight ($\sigma_v \gtrsim 100$ km s^{-1}). This is because when the line is strongly broadened the core of the line needs a larger column of gas to become optically thick, and so the linear branch of the growth curve spans over a larger range of N_{H} before saturating. From equations (2), (3), and (5), using the same numerical factor as in equation (8), and setting $\beta_{\sigma_v} = \sigma_v/c$, we get

$$\tau_0 \simeq 2.9(f_{\mathrm{lu}})_{0.5}(\xi_{\mathrm{X}i})_{0.4}(A_{\mathrm{X}})_{-5}A^{0.5}(\mathrm{N})_{22} \times [(T)_6 + A(2.3 \times 10^3\beta_{\sigma_v})^2]^{-0.5}E_0^{-1}\ . \tag{9}$$

In the above equation the two terms within the square brackets describe the contribution to the core optical depth by the two considered Doppler mechanisms. From equation (6) we know that dispersion velocities of the gas along the line of sight greater than ~ 100 km s^{-1} make the turbulence broadening mechanism very efficient compared to the thermal one and so reduce the core optical depth of each line. Equation (9) then allows definition and evaluation of the core optical depth in the two extreme cases: $\sigma_v = 0$ (thermal motion only, τ_0^{therm}) and $\sigma_v \gg (kT/M)^{1/2}$. We get

$$\tau_0^{\mathrm{therm}} \simeq 2.9(f_{\mathrm{lu}})_{0.5}(\xi_{\mathrm{X}i})_{0.4}(A_{\mathrm{X}})_{-5}A^{0.5}(\mathrm{N})_{22}(T)_6^{-0.5}E_0^{-1}\ , \tag{10}$$

$$\tau_0^{\mathrm{turb}} \simeq 1.24(f_{\mathrm{lu}})_{0.5}(\xi_{\mathrm{X}i})_{0.4}(A_{\mathrm{X}})_{-5}(\mathrm{N})_{22}(\beta_{\sigma_v})_{-3}^{-1}E_0^{-1}\ . \tag{11}$$

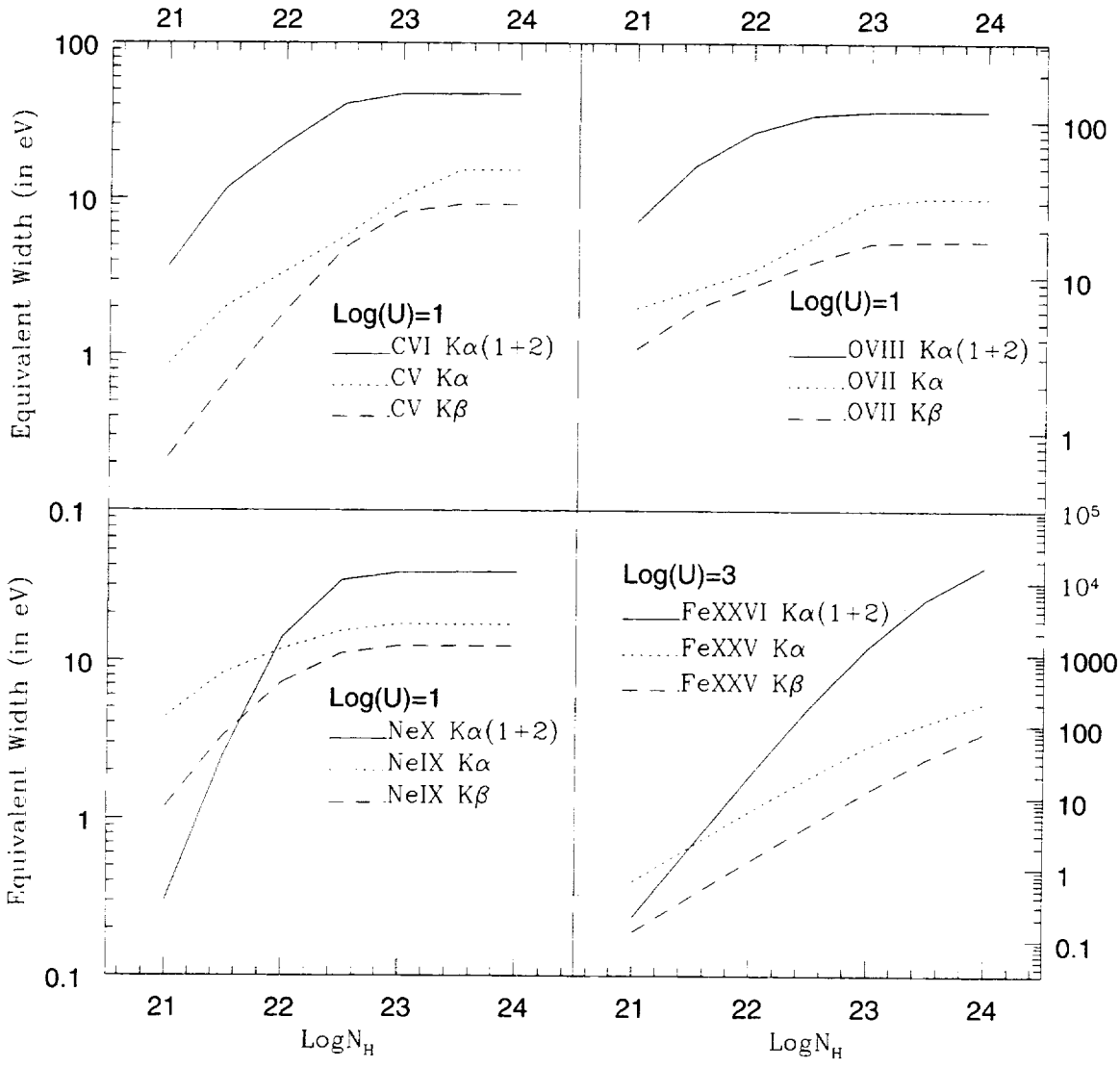

FIG. 2.—Same as Fig. 1, but for $\sigma_v = 1000$ km s^{-1}.

The ratio between these two quantities does not depend on the particular considered transition, the distribution of the ionic abundances in the gas, and its column density, and is therefore a good estimator of the relative contribution of the two Doppler broadening mechanisms to the core optical depth:

$$\frac{\tau_0^{\rm therm}}{\tau_0^{\rm turb}} = 2.3 A^{0.5}(T)_6^{-0.5}(\beta_{\sigma_v})_{-3} . \quad (12)$$

Equation (12) tells us that a given column of nonturbulent highly ionized gas in photoionization equilibrium can be more than a factor of 10 thicker to the resonant absorption process (at the energy of the transition) than an identical column of gas undergoing strong turbulence [$\sigma_v \gtrsim 300$ km s^{-1}, i.e., $(\beta_{\sigma_v})_{-3} \gtrsim 1$].

2.3. *Emerging X-Ray Spectra*

The relative importance of the spectral features in spectra emerging from photoionized gas obscuring the line of sight strongly depends on the spectral energy distribution of the ionizing continuum in the UV to X-ray energy range. We therefore treat separately the two extreme observed cases: (a) flat X-ray spectrum, broad optical emission-line type 1 AGN continua, and (b) steep X-ray spectrum, narrow optical emission-line type 1 AGN continua. If a peculiar class of AGNs does exist, with intrinsic UV to X-ray continuum switching between these two extreme observed cases (as suggested by the behavior observed in 1H 0419−577, Guainazzi et al. 1999, Turner et al. 1999; NGC 4051, Guainazzi et al. 1998; RE J2248−511, Puchnarewicz et al. 1995), then sources belonging to this class would show emerging spectra of the types (a) and (b) alternately.

2.3.1. *Flat X-Ray Ionizing Continuum*

Typical O-UV to X-ray continua of broad-line type 1 AGNs (i.e., $\alpha_E \sim 1$, $\alpha_{OX} \sim 1.3$) transmitted by photoionized gas show deep O VII–O VIII edges, since those are usually the most abundant oxygen ions. In these conditions, when the oxygen is mainly distributed in highly ionized states, carbon is almost fully stripped and neon is mostly distributed between Ne IX and Ne XI. Conversely, high-ionization iron ions are not much populated, the main ions being Fe XIV–Fe XX (Nicastro et al. 1999). In Figure 3, we show 0.1–5 keV

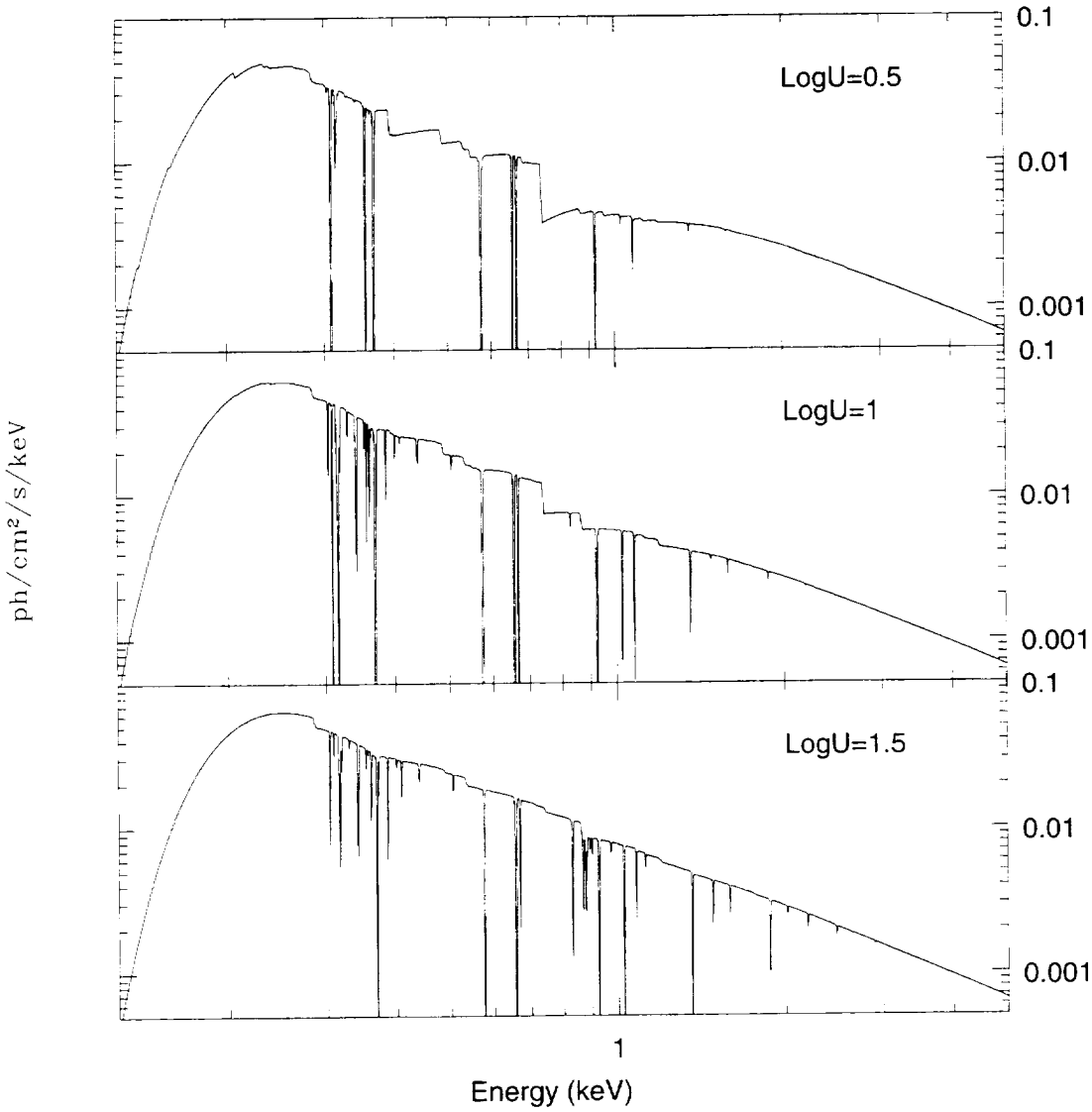

FIG. 3.—0.1–5 keV spectra emerging from an outflowing wind photoionized by a typical flat X-ray, broad-line type 1 AGN continuum, for log $U = 0.5$, 1, 1.5, $v_{out} = 1000$ km s^{-1}, $\sigma_v = 500$ km s^{-1}, and $N_H = 6 \times 10^{21}$ cm^{-2}. The low energy turnover is due to absorption from a column of neutral gas, to mimic typical Galactic absorption.

spectra emerging from an outflowing wind photoionized by a typical flat X-ray spectrum, broad optical emission-line type 1 AGN continuum (Ferland 1997), for three different values of log $U = 0.5$, 1, 1.5. We used an outflowing velocity of $v_{out} = 1000$ km s^{-1}, which is typical for the UV outflowing component in warm absorbers (Mathur et al. 1995) and which corresponds to $z = -0.003$. For the dispersion velocity, we adopted a value $\sigma_v = 500$ km s^{-1}. The column density of photoionized gas along the line of sight is fixed at $N_H = 6 \times 10^{21}$ cm^{-2}, which is the mean value in the Reynolds (1997) sample. We also added absorption from cold gas of column density $N_H^{Cold} = 3 \times 10^{20}$ cm^{-2} to simulate a typical Galactic absorption along the line of sight. In each panel of Figure 3 we plot the transmitted spectra corresponding to a given value of log U.

Moving from log $U = 0.5$ to log $U = 1.5$ (i.e., from low to high ionization, Fig. 3, *top to bottom*) the O VII K edge opacity decreases, due to the decreasing of the O VII/O VIII relative abundances ratio. Conversely the optical depth of the O VIII K edges increases until the O VII → O VIII photoionization rate becomes lower than the O VIII → O IX one. In Figure 3 (*bottom*) (log $U = 1.5$) only the O VIII K edge is visible, whereas the gas is almost completely transparent at the O VII K edge energy. In the lower ionization case (log $U = 0.5$; Fig. 3, *top*), a deep O VII K edge is instead present, along with the 0.49 keV K edge of C VI. Ne IX K edge is marginally visible because of the low column density adopted.

Strong O VII Kα and Kβ and O VIII Kα resonance absorption lines at 0.574, 0.653, and 0.665 keV, respectively, as well as C V, C VI, Ne IX, and Ne X Kα and Kβ lines, are present in these spectra with intensities and equivalent widths depending weakly on the ionization state. On the other hand, intensities and equivalent widths strongly depend on the dynamics of the absorbing clouds of gas along the line of sight and on its column density. For the case under consideration ($\sigma_v = 500$ km s^{-1}, $N_H = 6 \times 10^{21}$ cm^{-2}) the equivalent widths of Kα and Kβ He-like and H-like carbon, oxygen, and neon are in the range 2–8 eV. In the medium and higher ionization cases, Kα and Kβ lines from Mg and

Si are also present, along with two complex systems of S XI–S XV and Fe XV–Fe XX L lines around 0.3 and 1 keV, respectively. Their equivalent widths in the higher ionization case are of the order of 1 eV for each line. We note that the energies of the strong Kα and Kβ Ne IX and Ne X lines, as well as those of a number of Fe XVII and Fe XVIII lines, are all close to each other and to the energy of the O VIII K edge. Caution should then be used when fitting low- and medium-resolution spectra of warm absorbers with a phenomenological multiedge model. Neglecting the presence of this system of absorption lines (which may reach total equivalent width of up to a few tens of eV for σ_v = 1000 km s^{-1}) and leaving the optical depths of each edge free to vary independently in these fits may result in good fits from the χ^2 point of view, but in overestimating the O VIII optical depths.

2.3.2. *Steep X-Ray Ionizing Continuum*

When the ionizing continuum is steep below 2 keV ($\alpha_E \gtrsim 2$) and flattens above this energy to $\alpha_E \sim 0.7$–1.5, as in many NLSy1s, the resulting ionization structure can be quite different from the ones described in the previous section. In fact, in these condition C, O, and Ne would be almost fully stripped in the gas, whereas iron would still be distributed in medium–low ionization states, giving rise to emerging spectra with no sharp absorption features below $\sim$1 keV and a broad absorption structure between 1 and 2 keV due to a complex mixture of L resonance absorption lines and edges from Fe X–Fe XX.

As an example, Figure 4 shows two spectra emerging from an outflowing wind photoionized by a typical NLSy1 continuum (see Leighly et al. 1997), consisting of a blackbody with kT = 0.13 keV and a power law with α_E = 0.9. The relative normalization between the soft and the hard components is such that the ratio between the bolometric luminosity of the blackbody component and the 2–10 keV luminosity is $[L_{\rm Bol}({\rm BB})/L_{2-10}({\rm PL})] \simeq 10$ (a mean value in the Leighly et al. sample). We assume also in this case $v_{\rm out}$ = 1000 km s^{-1}, σ_v = 500 km s^{-1}, and a column density of $N_{\rm H}^{\rm Cold} = 3 \times 10^{20}$ cm^{-2} neutral gas to mimic a typical Galactic absorption. In Figure 4 (*top*) we plot the spectrum emerging from gas with log $U = -0.5$ and log $N_{\rm H}$ = 22. Both absorption lines and edges form the H-like and He-like ions of C, O, and Ne, along with a number of Si L lines around 0.3 keV, are imprinted on spectra emerging from photoionized gas with this (or lower) value of U, similar to what is found in the case of flat X-ray ionizing continuum; see Figure 3. Figure 4 (*bottom*) illustrates the

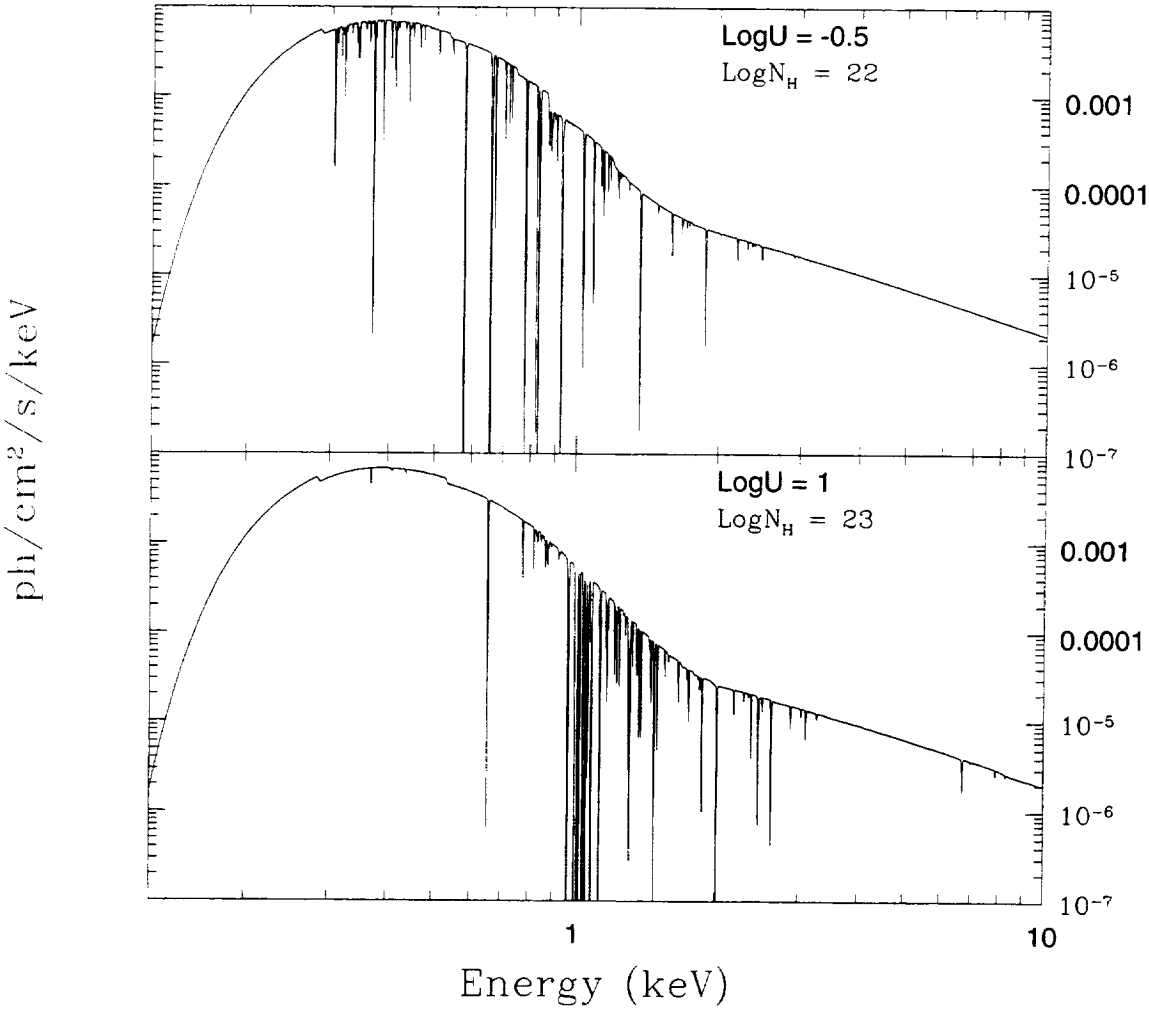

FIG. 4.—Spectra emerging from an outflowing wind photoionized by a typical NLSy1 continuum and with $v_{\rm out}$ = 1000 km s^{-1} and σ_v = 500 km s^{-1}. The ionizing continuum used consists of a blackbody with kT = 0.13 keV and a power law with α_E = 0.9. The ionization parameter and gas column density are log $U = -0.5$, log $N_{\rm H}$ = 22 and log U = 1, log $N_{\rm H}$ = 23 in the upper and lower panels, respectively.

case of a much higher ionization (log $U = 1$). Here we use a column density an order of magnitude higher than in the previous case to highlight the peculiarities of this model: no deep absorption edge is visible in this spectrum, despite the very high column density of $N_H = 10^{23}$ cm^{-2}, whereas a complex system of strong absorption lines between 1 and 2 keV is clearly visible, due to almost 60 L lines of midionized iron and Kα and Kβ lines of Mg, Si, and S. The iron L lines around 1 keV are all very close in energy, and their equivalent widths span from a few eV for $\sigma_v = 500$ km s^{-1} up to tens of eV for $\sigma_v = 1000$ km s^{-1}. The total equivalent width due to these lines between 1 and 1.5 keV can be as high as a few hundred eV.

Let us now suppose that the ionized gas in NLSy1 has physical properties similar to the warm absorbers in flat X-ray spectrum type 1 AGNs, i.e., similar electron density and similar distance to the source of the ionizing radiation in units of gravitational radii. Pounds et al. (1995) and Laor et al. (1997) suggested that steep X-ray spectrum, narrow-line quasars are emitting close to the Eddington luminosity, at a rate, say, a factor of 10 higher than flat X-ray spectrum broad-line quasars. This means that the black hole mass of steep X-ray quasars is a factor of 10 smaller than that of flat X-ray quasars with a similar luminosity (in agreement with variability studies, Fiore et al. 1998a, and with detailed modeling of the optical UV X-ray SED of NLSy1s, Puchnarewicz, Mason, & Siemiginowska 1998). The remarkable uniformity of ionization parameters found by Reynolds (1997) and George et al. (1998) in their samples of Seyfert 1 galaxies and quasars of luminosity spanning 3 orders of magnitude implies that the product $R^2 n_e$ scales linearly with the luminosity in these objects. If this correlation holds for NLSy1s too, then we can estimate the $R^2 n_e$ factor of a NLSy1 of a given luminosity using, for example, the Reynolds estimate but scaling the distance between the absorber and the ionizing source by the above factor of 10. For a NLSy1 of luminosity 10^{43} ergs s^{-1} we find $R^2 n_e \sim 10^{40}$ cm^{-1}, using the typical ionization parameter found by Reynolds (1997). Using this value and the correct ionizing continua we expect for a typical NLSy1 a log U of 0.8–1.2 and therefore a spectrum similar to that plotted in Figure 4 (*bottom*).

3. DATA AND SIMULATIONS

To compare our models with the available data and to make predictions on what we will be able to observe with the next generation of X-ray spectrometers (i.e., gratings and calorimeters), we folded our photoelectric plus resonant absorption model with the responses of the *ASCA* SIS, *AXAF* ACIS/HETG, and a high-resolution, high effective area calorimeter as the baseline for the future mission Constellation-X. The simulations were performed using model parameters as deduced from the *ASCA* data of the Seyfert 1 galaxy NGC 985 and the NLSy1 IRAS 13224−3809. We discuss these two cases in turn.

3.1. *Flat Ionizing Continuum: The Case of NGC 985*

NGC 985 is a Seyfert 1 galaxy known to host an ionized absorber (Brandt et al. 1994). Nicastro et al. (1998) observed the source with *ASCA* and confirmed the presence of an ionized absorber along the line of sight. They find that a single-zone photoionization model (accounting for photoelectric absorption only, model *a*) is not able to explain completely the complex absorption structure seen in the *ASCA* spectrum (the continuum has been parameterized as a power law with $\alpha_E = 1.3$ up to 2.3 keV, whereas above this energy the spectrum flattens by $\Delta\alpha_E = 0.6$, the ionized absorber parameters are log $U = 0.93 \pm 0.09$, log $N_H = 21.95 \pm 0.05$, and $z_{abs} = 0.023^{+0.034}_{-0.029}$, which implies a maximum outflowing velocity $\approx 15{,}000$ km s^{-1}). Analysis of the *ASCA* SIS residuals shows a significant deficit of counts around ~ 1 keV (Fig. 5*a*). The equivalent width of this feature (estimated by adding a Gaussian absorption line to the continuum model) is $-(13 \pm 4.0)$ eV.

We computed the spectrum emerging from gas photoionized by the NGC 985 optical to X-ray continuum using our photoelectric plus resonant absorption model. We extrapolated the soft X-ray power law, as measured from the *ASCA* data, through optical wavelengths. This is consistent with both the measured O-UV spectral index $\alpha_{O\text{-}UV} = 1.4$ (de Vaucouleurs et al. 1991) and $\alpha_{OX} = 1.4$. We adopted for log U and log N_H the best-fit values given above and an outflowing velocity of 1000 km s^{-1}, which is the mean measured value for the known O-UV/X-ray ionized absorbers (Mathur et al. 1994, 1995, 1997, 1998) and is consistent with the estimate of the warm absorber redshift in this source. We used a dispersion velocity of 1000 km s^{-1}. The model is plotted in Figure 5*c*. It shows strong resonance absorption lines between 0.85 and 1.2 keV due to the redshifted Kα and Kβ Ne IX and Kα Ne X lines. The blend of these three lines has a total equivalent with of about 20 eV, similar to the equivalent width of the line feature in Figure 5*a*. We folded this model with the *ASCA*-SIS response and simulated a 40 ks observation of NGC 985. We fitted the resulting spectrum with model *a*. The ratio between the simulation and best-fit model *a* is shown in Figure 5*b*; it resembles strikingly the residuals to the "real" spectrum in Figure 5*a*. Although this is certainly not a self-consistent, quantitative, and unique description of the spectrum of NGC 985, it indicates that resonant absorption may well be the cause of the feature observed at about 1 keV.

The spectrum in Figure 5*c* also shows strong absorption Kα and Kβ lines from O VII and O VIII at 0.57 and 0.65 keV. There is no evidence for an absorption feature (in addition to photoelectric absorption) at these energies in the *ASCA* spectrum of NGC 985 (Fig. 5*a*). Contribution from emission lines due to recombination could be important at these energies, and so they could help in reducing the depth of the absorption lines. Line emission strongly depends on the covering factor, and therefore an accurate estimate of line emission intensity can provide information on the geometry and distribution of the ionized gas. However, the above energy is close to the lower threshold of the SIS instrument, where the calibration is most uncertain and problems due to the residual dark distribution (RDD) are large, and where the CCD energy resolution is 5–6 only. For a quantitative study of the O VII and O VIII emission/absorption lines we should await instruments with better energy resolution and coverage.

As a next step we folded the photoelectric plus resonant absorption model of Figure 5*c* with the responses of *AXAF* ACIS/HETG and the baseline Constellation-X calorimeter, which has a factor of 2 worse energy resolution but a factor of 100 higher effective area (at 1 keV). The simulations are shown in Figures 6*a*, 6*b*, 6*c* and 7*a*, 7*b*, 7*c* for three different values of the dispersion velocity: $\sigma_v = 100$, 500, and 1000 km s^{-1} for panels (*a*), (*b*), and (*c*), respectively. The first-order *AXAF* ACIS/MEG (medium energy grating) simula-

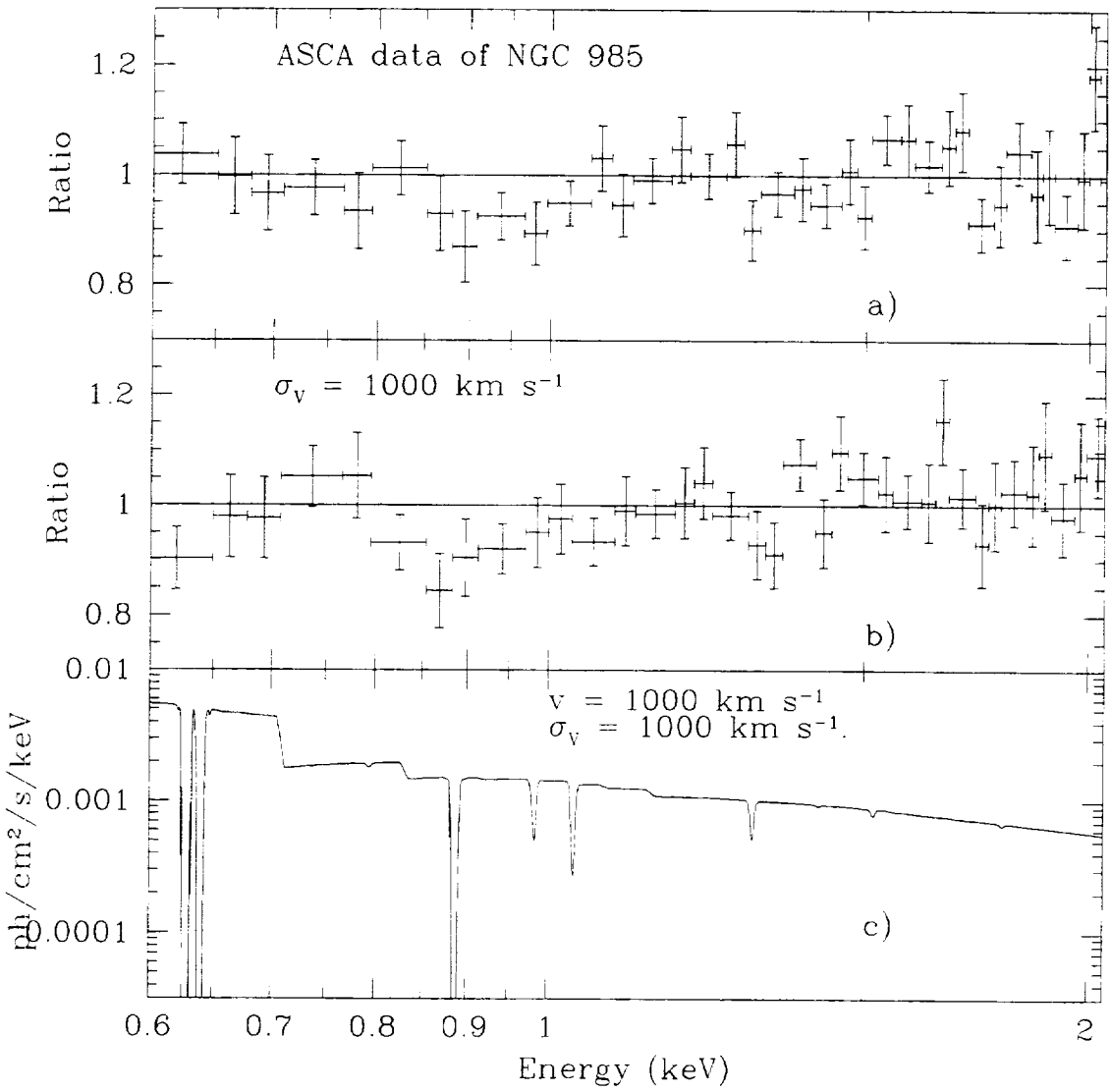

FIG. 5.—(*a*) Ratio between the co-added *ASCA* SIS0 and SIS1 data of NGC 985 and the best-fitting model *a*. (*b*) Ratio between a 40 ks *ASCA* SIS simulation, obtained using the model plotted (*bottom*; see text for details), and model *a*. (*c*) The spectrum emerging from gas photoionized by the NGC 985 SED, when accounting for both photoelectric and resonant absorption. We adopted outflowing and dispersion velocities of 1000 km s^{-1}.

tions (Fig. 6) were performed using the MARX simulator (Wise et al. 1997, MARX User Guide, version 1.0[8]). The exposure time is 80 ks. To simulate the calorimeter spectrum (Fig. 7), we wrote a simple program to fold our models with the response matrix[9] and add statistical noise. The exposure time in the Constellation-X calorimeter simulations is 10 ks.

Resonance absorption lines of width $\gtrsim$200 km s^{-1} are detected in the *AXAF* ACIS/HETG first-order spectrum. All the strongest lines in Figure 5*c* are resolved in the spectra of Figures 6*b* and 6*c*. *AXAF* HETG spectra of Seyfert 1 galaxies will then establish whether resonant absorption is important in the ionizing gas and then provide estimates of the gas dispersion velocity and bulk motion. This will allow unambiguous solution of the open and controversial issue on the identification between the X-ray and the UV ionized absorbers. However, the signal to noise will be poor in most cases: the O VII Kα/Kβ and Ne IX Kα/Kβ line ratios, which can be used for plasma diagnostic, cannot be estimated with uncertainty $\lesssim$100%; line widths and profiles that give information on the geometrical and dynamical configuration of the absorber can be roughly measured but not studied in detail. The HETG can obtain spectra of comparable quality for about 100 AGNs.

The large effective area of the Constellation-X calorimeter along with a good energy resolution will permit attainment of high signal-to-noise spectra, of a quality similar to optical spectra of AGNs, of sources of the brightness of NGC 985. This will allow application of plasma diagnostics, accurate measurement of both the chemical composition and ionic distribution of the gas, discrimination between collisional ionization and photoionization, and study of the time-evolving behavior of the relevant physical quantities

[8] http://asc.harvard.edu/prop_port.html#marker_marx.
[9] ftp://legacy.gsfc.nasa.gov/htxs/calor_w_grat.rsp.gz.

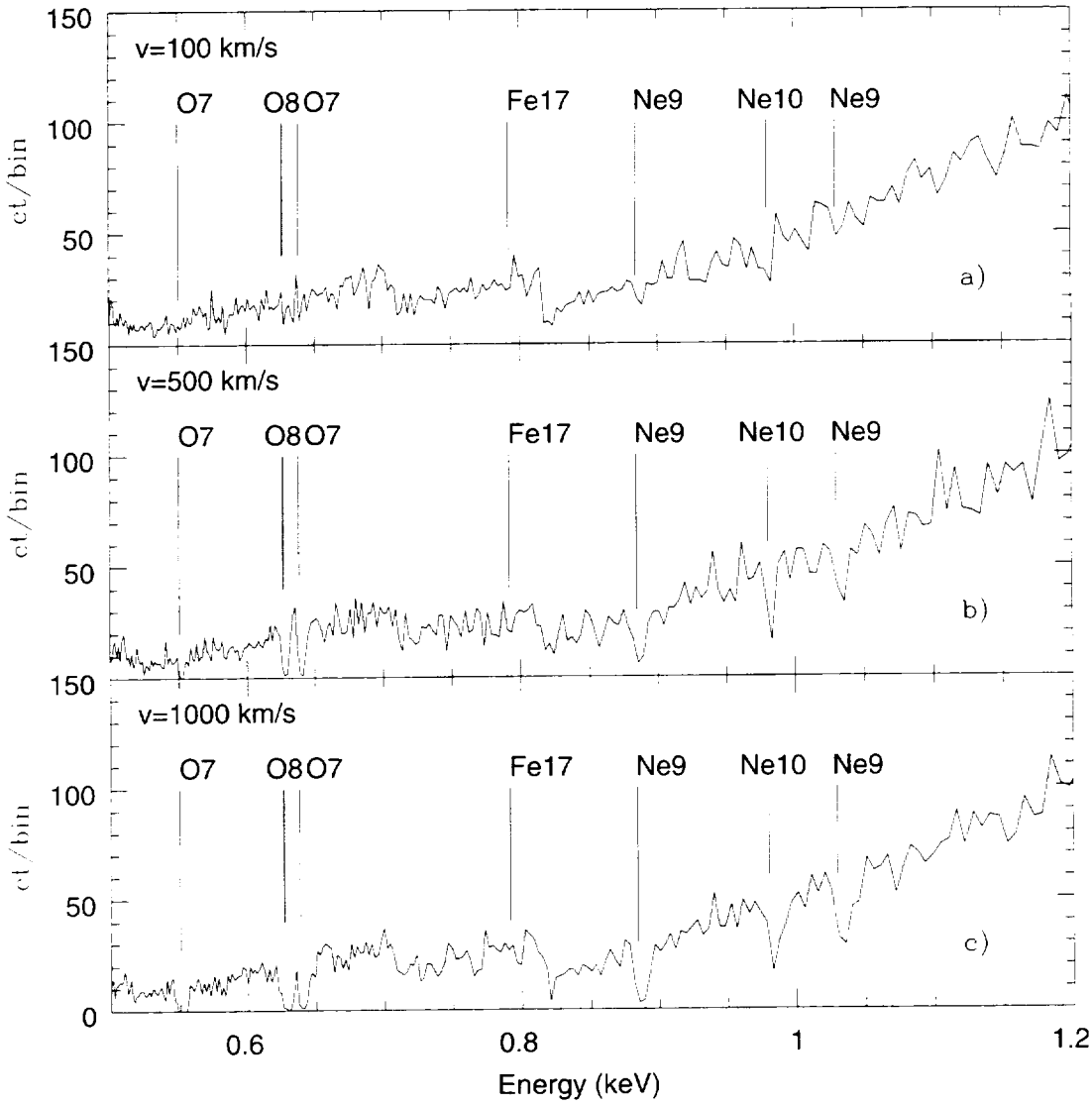

FIG. 6.—Simulations of 80 ks 0.4–1.2 keV first-order *AXAF* ACIS/MEG spectra of NGC 985. A dispersion velocity of σ_v = 100, 500, and 1000 km s^{-1} has been used in (*a*), (*b*), and (*c*), respectively.

(temperature, relative ionic abundances, etc.), which in turn will allow constraint of important physical and geometrical parameters (electron density and radial distance; Nicastro et al. 1999). The Constellation-X calorimeter could provide moderate signal-to-noise spectra, similar to those in Figure 6, of sources down to a flux limit of a few 10^{-13} ergs cm^{-2} s^{-1}, which increases the sample of possible targets to a few tens of thousand sources. AGNs with luminosity in the range 10^{43}–10^{44} ergs s^{-1} can be studied up to $z = 0.3$–0.5, whereas more luminous (10^{46}–10^{47} ergs s^{-1}) quasars will be available up to $z \sim 3$ (the limit is given by the bandwidth of the Constellation-X calorimeter more than by its sensitivity, since features at 0.5–1 keV are redshifted to 0.12–0.25 keV for $z = 3$). This will permit the study of the evolution of physical state, chemical composition, and geometry of the absorbing gas with redshift and luminosity. Statistical studies on the distribution of the absorber density, ionization state, chemical composition, and distance from the ionizing source will be possible, which can give information on the absorber origin.

3.2. *Steep Ionizing Continuum: The Case of IRAS 13224−3809*

We chose to test our model on the NLSy1 galaxy IRAS 13224−3809, which showed in an *ASCA* observation a deep absorption feature in the interval 1–2 keV, interpreted by Leighly et al. (1997) in terms of resonant absorption from gas outflowing with $v/c \sim 0.5$

Figure 8*a* shows the ratio between the co-added *ASCA* SIS0 and SIS1 data and the best-fitting model composed by a blackbody plus a power law, with best-fit parameters given by $kT = 0.134$ keV, $\alpha_E = 1.16$, and $[L_{\rm Bol}({\rm BB})/L_{2-10}({\rm PL})] = 9.8$ (fully consistent with both the Leighly et al. 1997 and the Hayashida 1997 estimates). A deep and broad deficit of counts is evident between 0.9 and 2 keV (also see Fig. 1 in Leighly et al. 1997). The absorption feature equivalent width (estimated by adding a Gaussian absorption line to the continuum model) is large: EW = $-(180 \pm 30)$ eV. We note that, even if the deficit of counts occurs approximately where the blackbody and the

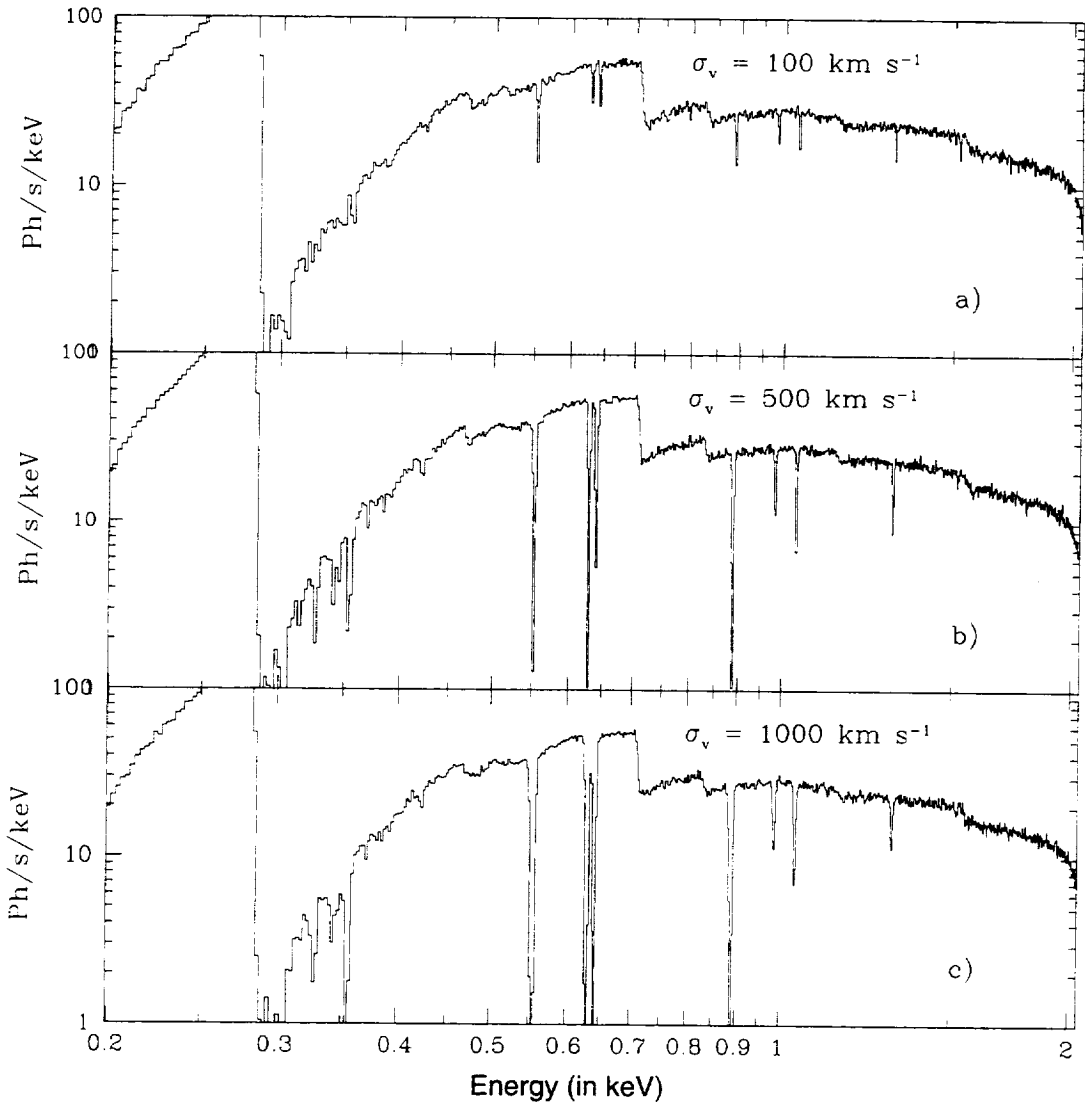

FIG. 7.—Simulations of 10 ks spectra of NGC 985 taken with the Constellation-X calorimeter. A dispersion velocity of σ_v = 100, 500, and 1000 km s^{-1} has been used in (*a*), (*b*), and (*c*), respectively. The cutoff at low energy is partly due to the inclusion at low energy of neutral absorption from the Galactic column along the line of sight ($N_H = 3 \times 10^{20}$ cm^{-2}).

power-law components match each other, we were not able to model the absorption-like feature without invoking a third component.

We computed the spectrum emerging from gas photoionized by the IRAS 13224−3809 UV to X-ray continuum for a number of values of log U (from −0.5 to 1.5), log N_H (from 10^{22} to 10^{24} cm^{-2}), and σ_v (from 100 to 1000 km s^{-1}). We extrapolated down to 13.6 eV and up to 100 keV the best-fit continuum to the *ASCA* data of IRAS 13224−3809. This is in good agreement with the optical UV to X-ray measures of this source, which suggests that the thermal disk component in this object could be present at higher energies than usually found in soft X-ray flat, broad-line type 1 AGNs (Mas-Hesse et al. 1994). We adopted for the hard X-ray power law the best-fit spectral index $\alpha_E = 1.16$. This value is in excellent agreement with the mean estimate of Hayashida (1997). However, as Brandt et al. (1997) pointed out, the spectral index of the hard power law of IRAS 13224−3809 is highly variable, ranging between 0.7 and 1.3. The value that we used in our model represents therefore only a mean value. We stress however that the exact shape of the hard power law does not affect strongly the distribution of the relative ionic abundances in the gas for elements lighter than neon, which is instead mainly driven by the presence of a strong soft excess below ~2 keV. Our results are therefore rather insensitive to the exact slope of the hard power law. As in the previous case we adopted an outflowing velocity of 1000 km s^{-1}. We folded these models with the *ASCA*-SIS response and then fitted them with a blackbody plus power-law model. As an example Figure 8*b* shows the ratio between an 80 ks simulation obtained using log $N_H = 23.5$, log $U = 1$, outflowing and dispersion velocities of 1000 km s^{-1} (model shown in Fig. 8*c*), and the best-fitting blackbody plus power-law model. We note that all the relevant absorption lines lie in a spectral region in which the intrinsic continuum is still dominated by the soft blackbody component (Fig. 8*c*, but see also Fig. 4). The residuals resemble those in Figure 8*a*. The large deficit of counts between 0.9 and 2 keV is due to the presence of a large number of iron L lines. The co-added equivalent width

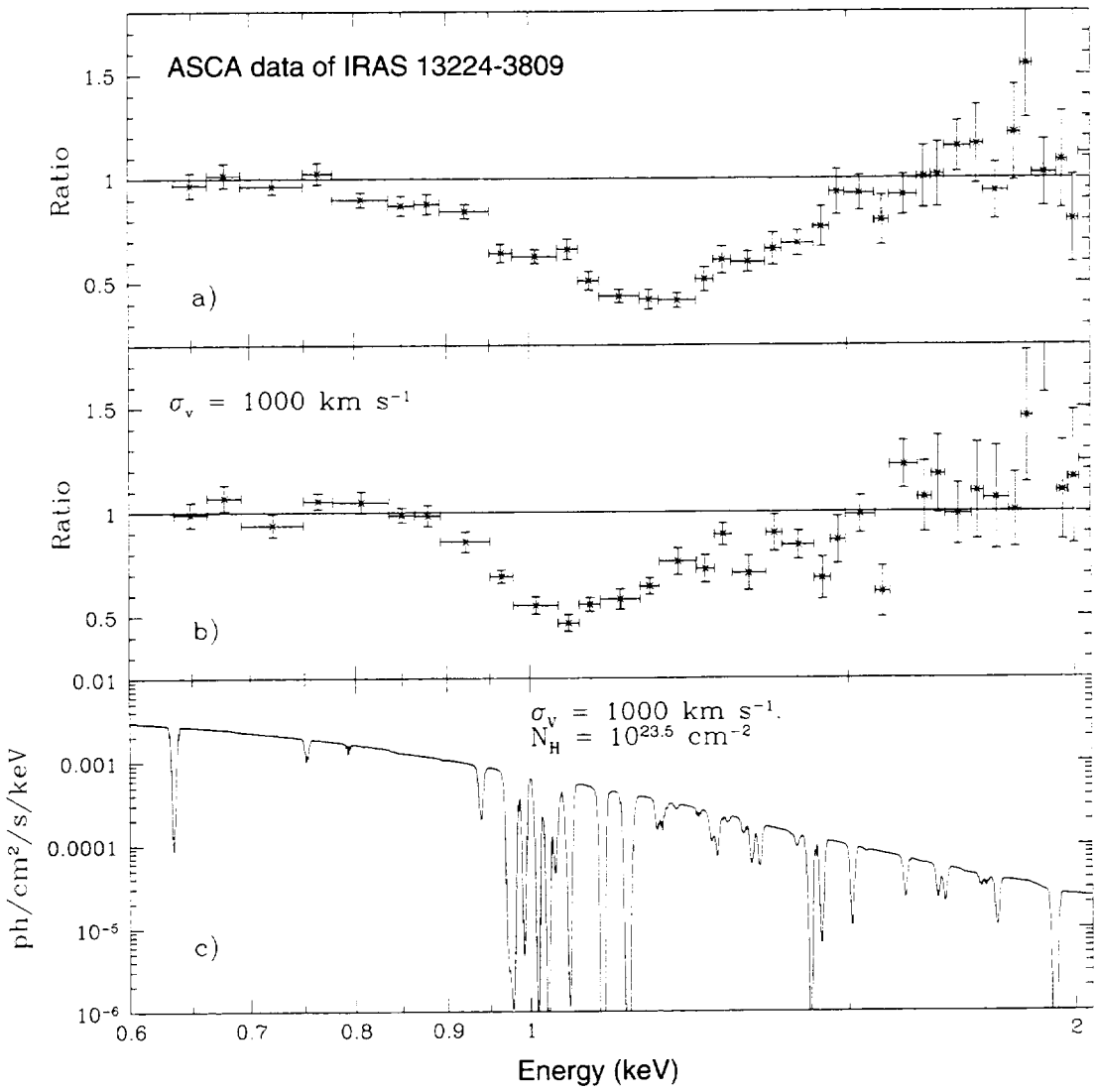

FIG. 8.—(*a*) Ratio between the co-added *ASCA* SIS0 and SIS1 data of IRAS 13224−3809 and the best-fitting blackbody plus power-law model. (*b*) Ratio between a 80 ks *ASCA* SIS simulation, obtained using the model plotted (*bottom*; see text for details) and the best-fitting blackbody plus power-law model. (*c*) The spectrum emerging from gas photoionized by the IRAS 13224−3809 SED, when accounting for both photoelectric and resonant absorption. We adopted outflowing and dispersion velocities of 1000 km s^{-1}.

of these lines is about 130 eV, similar to the equivalent width of the absorption feature in Figure 8*a*.

As for the case of NGC 985, we plot in Figures 9*a*, 9*b*, 9*c* and 10*a*, 10*b*, 10*c* three simulations obtained convolving the spectrum in Figure 8*c* with the *AXAF*/MEG and Constellation-X calorimeter responses. The simulations are shown for three values of the dispersion velocity, σ_v = 100, 500, and 1000 km s^{-1} (Figs. 10*a*, 10*b*, and 10*c*, respectively). Integration time was 100 ks for the first-order *AXAF*/MEG spectrum and 20 ks for the Constellation-X calorimeter spectrum.

Many single Fe L lines are well resolved even in spectra with dispersion velocity of 1000 km s^{-1}. *AXAF*/HETG spectra of low-redshift NLSy1s with luminosity $L = 10^{43}$–10^{44} ergs s^{-1} will permit unambiguous establishment of whether an ionized absorber is indeed responsible for the 1 keV deficit of counts seen in many moderate-resolution X-ray spectra of these sources. The low signal-to-noise ratio of *AXAF*/HETG spectra, however, will not allow application of plasma diagnostics to infer the physical properties of the absorbers. Nevertheless the outflowing and dispersion velocities of the gas will be accurately derived, as well as the relative Ne to O and Fe to Si and Mg abundances, which will put important constraints on the geometry and the chemical composition in the AGN environment. The high effective area of the Constellation-X calorimeter will allow a great increase of the sample of narrow-line type 1 AGNs observed at high resolution. The complex iron L edges and line absorption system could be detected in high-luminosity narrow-line quasars up to redshift $\lesssim 2$, or even higher, depending on the actual response below the carbon edge (0.283 keV), whereas Mg and Si Kα and Kβ resonance absorption lines could be detected up to $z \sim 3$. The good energy resolution (3 eV), will permit separation of the strongest (oscillator strength greater than 0.05) single resonance absorption lines of the 1 keV iron L edge plus line complex, thus allowing for a clear diagnostic of the mechanism responsible for the ionization of the gas. In particular,

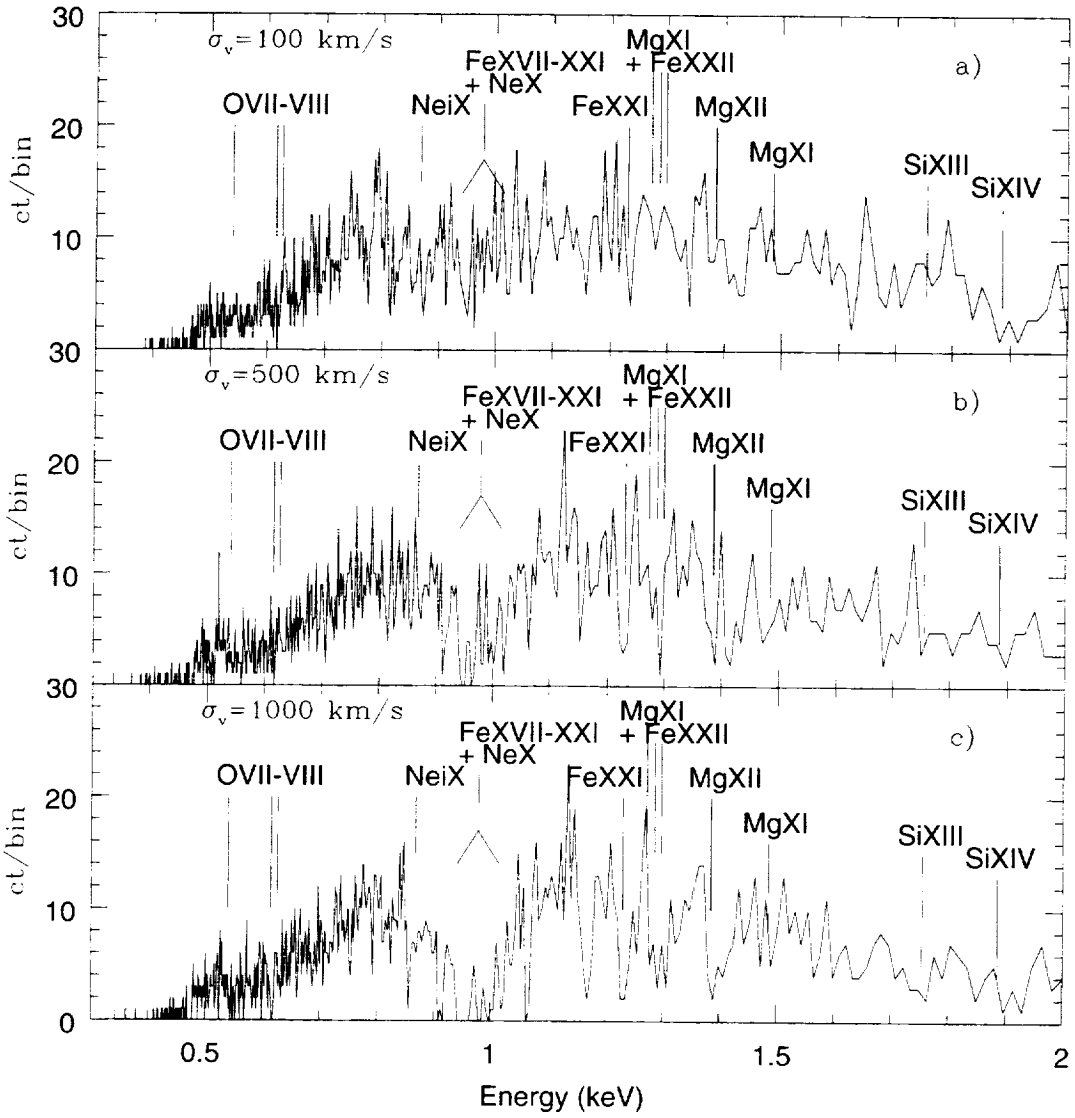

FIG. 9.—Simulations of 100 ks 0.4–2 keV first-order *AXAF* ACIS/MEG spectra of IRAS 13224−3809. A dispersion velocity of σ_v = 100, 500, and 1000 km s^{-1} has been used in (*a*), (*b*), and (*c*), respectively.

an accurate measure of the relative abundances of the very stable Fe XVII Li-like ion could allow clear distinction between gas in collisional or photoionization equilibrium (Nicastro et al. 1999). Time-evolving ionization can also be investigated, thus giving constraints on the electron density and the radial distance of the absorbers (Nicastro et al. 1999).

4. CONCLUSIONS

We have calculated spectra emerging from ionized gas taking into account both photoelectric and resonant absorption. We find that the emerging spectra are strongly modified by resonant absorption if the dispersion velocity in the gas is $\gtrsim$100 km s^{-1}. This, or even higher values, is not unrealistic, since many broad-line AGNs show absorption lines in the UV blueshifted by 200–2000 km s^{-1} and broadened by similar dispersion velocities.

In particular we find the following.

1. The distribution of relative ionic abundances in photoionized gas dramatically depends on the exact shape of the ionizing continuum.

2. Strong Kα and Kβ resonance absorption lines from He-like and H-like ions of C, O, and Ne, along with deep C VI, O VII–O VIII, Ne IX–Ne X K edges, and Fe XV–Fe XVII L edges, are expected to be present in the 0.1–3 keV spectra of flat X-ray spectrum quasars emerging from photoionized gas along the line of sight. When fitting low- and medium-resolution X-ray data with phenomenological multiedge models, these resonance absorption lines may produce the effect of overestimating the optical depth of the O VIII K edge.

3. Conversely, no strong absorption edge is expected to be imprinted on spectra emerging from gas illuminated by steep ionizing continua, with physical and geometrical properties similar to those found in broad-line type 1 AGNs. However, a large number of strong Fe L, Mg, Si, and S Kα and Kβ resonance absorption lines (almost 70) are predicted between 1 and 2 keV. Fitting low- and medium-energy resolution data with continuum models may then result in deep smooth negative residuals at these energies. We then suggest that the $\sim$1 keV absorption feature observed by *ASCA* in several narrow-line Seyfert 1 galaxies can be explained in terms of resonance absorption lines,

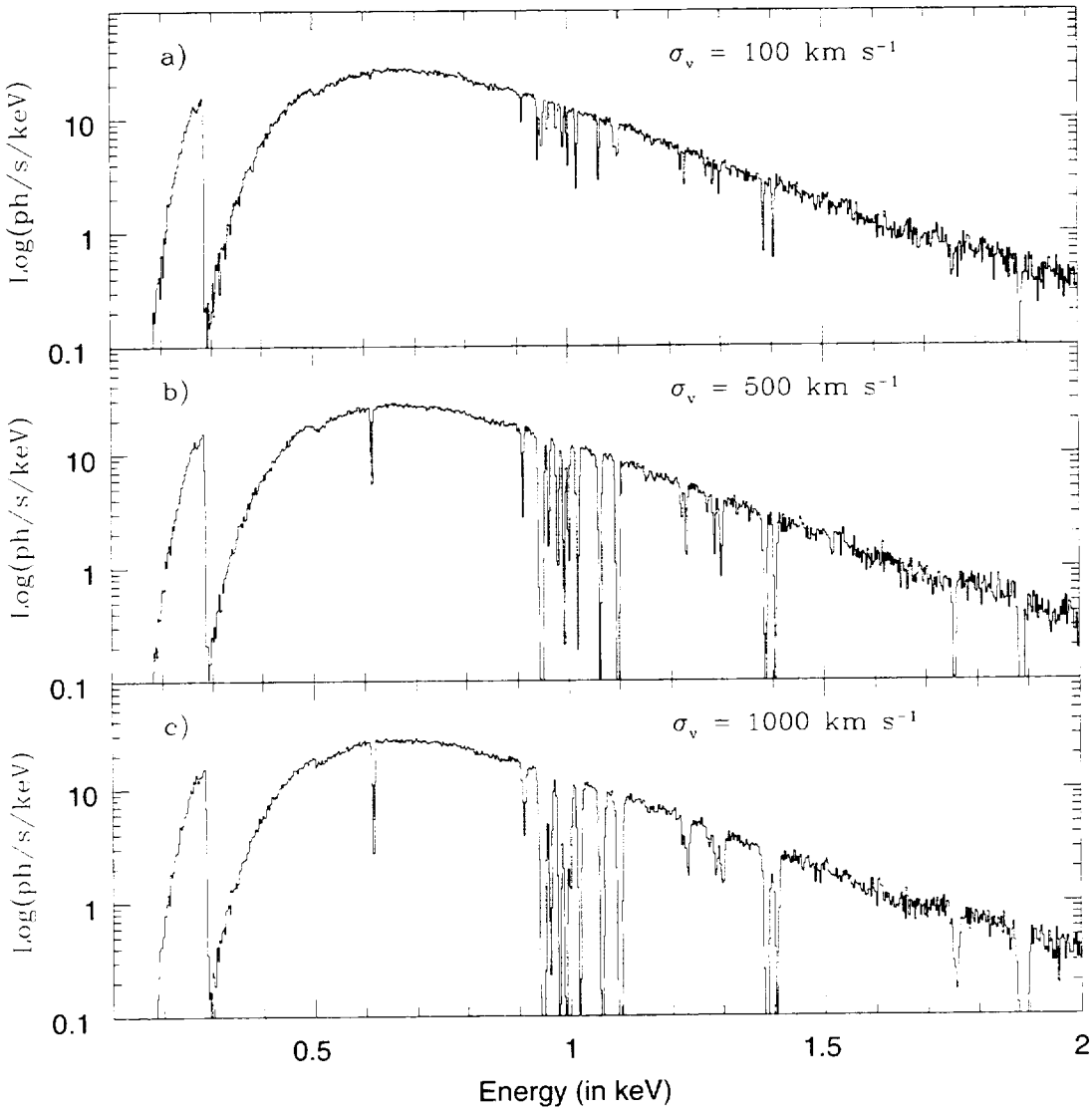

FIG. 10.—Simulations of 20 ks 0.3–2 keV spectra of IRAS 13224−2809 taken with the Constellation-X calorimeter. A dispersion velocity of σ_v = 100, 500, and 1000 km s^{-1} has been used in (*a*), (*b*), and (*c*), respectively. The cutoff at low energy is partly due to the inclusion of neutral absorption from the Galactic column along the line of sight ($N_H = 4.8 \times 10^{20}$ cm^{-2}).

without requiring relativistic outflowing velocities of the gas.

4. The equivalent width of the predicted resonant absorption lines strongly depends on the column density of the absorbing gas and its dispersion velocity. Assuming the range of N_H typically observed and dispersion velocities of 0–1000 km s^{-1}, we estimate equivalent widths spanning from a few eV to a few hundred eV.

F. F. acknowledges support from NASA grants NAG5-2476 and NAG5-3039.

REFERENCES

Boller, Th., Brandt, W. N., & Fink, H. 1996, A&A, 305, 53
Brandt, W. N. 1995, Ph.D. thesis, Univ. Cambridge
Brandt, W. N., Fabian, A. C., Nandra, K., Reynolds, C. S., & Brinkmann, W. 1994, MNRAS, 271, 958
Brandt, W. N., Mathur, S., & Elvis, M. 1997, MNRAS, 285, L25
de Vaucouleurs, G., et al. 1991, RC3.9, Vol. P
Ferland, G. J. 1997, CLOUDY Version 90.04
Fiore, F., Elvis, M., McDowell, J. C., Siemiginowska, A., & Wilkes, B. J. 1994, ApJ, 431, 515
Fiore, F., Laor, A., Elvis, M., Nicastro, F., & Giallongo, E. 1998a, ApJ, 503, 607
Fiore, F., et al. 1998b, MNRAS, 298, 103
George, I. M., Turner, T. J., Netzer, H., Nandra, K., Mushotzky, R. F., & Yaqoob, T. 1998, ApJS, 114, 73
Guainazzi, M., et al. 1998, MNRAS, 301, 1
———. 1999, A&A, in press
Hayashida, K. 1997, in ASP Conf. Ser. 113, Emission Line in Active Galaxies: New Methods and Techniques, ed. B. M. Peterson, F.-Z. Cheng, & A. S. Wilson (San Francisco: ASP), 40
Kriss, G. A., Espey, B. R., Krolik, J. K., Tsvetanov, Z., Zheng, W., & Davidsen, A. F. 1996a, ApJ, 467, 622
Kriss, G. A., et al. 1996b, ApJ, 467, 629
Krolik, J. H., & Kriss, G. A. 1995, ApJ, 447, 512 (erratum 456, 909 [1996])
Laor, A., Fiore, F., Elvis, E., Wilkes, B. J., & McDowell, J. C. 1997, ApJ, 477, 93
Leighly, K. M., Mushotzky, R. F., Nandra, K., & Foster, K. 1997, ApJL, 489, 25
Mas-Hesse, J. M., Rodriguez-Pascual, P. M., De Cordoba, L. S. F., & Boller, Th. 1994, A&A, 283, 9
Mathur, S., Elvis, M., & Wilkes, B. J. 1995, ApJ, 452, 230
Mathur, S., Wilkes, B. J., & Aldcroft, T. 1997, ApJ, 478, 182
Mathur, S., Wilkes, B. J., & Elvis, M. 1998, ApJ, 503, 23

Mathur, S., Wilkes, B. J., Elvis, M., & Fiore, F. 1994, ApJ, 434, 493
Matt, G. 1994, MNRAS, 267, L17
Matt, G., Brandt, W. N., & Fabian, A. C. 1996, MNRAS, 280, 823
Matt, G., et al. 1999, in preparation
Netzer, H. 1993, ApJ, 411, 594
———. 1996, ApJ, 473, 781
Nicastro, F., Fiore, F., Brandt, W., & Reynolds, C. S. 1998, The Active X-Ray Sky, ed. L. Scarsi, H. Bradt, P. Giommi, & F. Fiore (Amsterdam: Elsevier), 501
Nicastro, F., Fiore, F., Perola, G. C., & Elvis, M. 1999, ApJ, 512, 184
Pfefferman, E., et al. 1987, Proc. SPIE, 733, 519
Pounds, K. A., Done, C., & Osborne, J. P. 1995, MNRAS, 277, L5
Puchnarewicz, E. M., Branduardi-Raymond, G., Mason, K. O., & Sekiguchi, K. 1995, MNRAS, 276, 1281
Puchnarewicz, E. M., Mason, K. O., & Siemiginowska, A. 1998, MNRAS, 293, 52
Reynolds, C. S. 1997, MNRAS, 287, 513
Rybicky, G. B., & Lightman, A. P. 1979, Radiative Processes in Astrophysics (New York: Wiley)
Trümper, J. 1983, Adv. Space Res., 2(4), 241
Turner, T. J., et al. 1999, ApJ, 510, 178
Verner, D. A., Verner, E. M., & Ferland, G. J. 1996, At. Data Nucl. Data Tables, 64, 1
Walter, R., & Fink, H. 1993, A&A, 274, 105
Wise, M. W., Davis, J. E., Huenemoerder, D. P., Houck, J. C., Dewey, D., Flanagan, K. A., & Baluta, C. 1997, MARX User Guide, Version 1.0